ADDIS ABABA UNIVERSITY

ADDIS ABABA INSTITUTE OF TECHNOLOGY

SCHOOL OF MECHANICAL AND INDUSTRIAL ENGINEERING

Thermo-Mechanical Analysis of Railway Wheel – Rail Rolling/Sliding contact

A master's thesis Submitted to the Graduate School of Addis Ababa University in Partial Fulfillment of the Requirements for the Degree of Masters of Science in Railway Engineering (Rolling Stock)

By

Rebira Wirtu

Advisor

Mr. Habtamu Tekubet (Msc)

June 2017

Addis Ababa University

Addis Ababa Institute of Technology

School Of Mechanical and Industrial Engineering

Thermo-Mechanical Analysis of Railway Wheel – Rail Rolling/Sliding contact

APPROVAL BY BOARD OF EXAMINERS

	Signature	Date
1. Head, Railway Center Daniel Tilahun (Dr.)	……	. ……..
2. Advisor Habtamu Tekubet (Msc.)	……..	…….
3. Internal Examiner Yilma Tadese (Dr.)	…….	……..
4. External Examiner Haileleoul Sahle (Msc)	……..	…….

DECLARATION

I declare that the thesis for the M.Sc. degree at the university of Addis Ababa, hereby submitted by me, is my original work and has not previously been submitted for degree at this or any other university, that all resources of materials used for this thesis have been duly acknowledged.

Name: Rebira Wirtu

Signature: _____

Date of submission: _____

This thesis has been submitted for examination with my approval as a university advisor.

Name: Mr. Habtamu Tekubet

Signature: _____

Date: _____

ACKNOWLEDGEMENT

First and foremost, I am very grateful to God for keeping me blessed and granting me the ability to achieve my goal. This thesis would not have been possible without the generous support and encouragement of my advisor, Mr. Habtamu Tekubet. for his sustainable and appreciable guidance, tireless advising, for sharing his knowledge, skill ,experience and fine-tuning up to the successful completion of this thesis.., In addition, I am grateful to Ethiopian Railways Corporation (ERC) for their giving me such like opportunity and supporting me in finance. I would like to take this opportunity to thank my lovely mother who always believed in my ability to be successful in academic arena – too unfortunate she cannot see my graduate, your memory will be from my internal. My sincere thanks also goes to all my brothers and sisters who have been always besides me, helping me psychologically, emotional, physically and materially to over-come all the obstacles I faced during my life. Thanks to them I arrive to this level and I will remain always grateful toward them for what they have been doing. Moreover, I would like to express my heartfelt appreciation and thank to my Advisor Belay Woldeyes (Professor) Equally thanks goes to all of my dearest colleagues specially Gemechu B., Tamitrat E., Teshale T. Gadisa M., Gadisa D.,Tesfaye T. and JAERC for their cooperation and supporting me.

Thank you all!!! You are the best!!! Sincerely yours!!!

ABSTRACT

Thermal damage caused by frictional heat of rolling-sliding contact is one of the most important failure forms of wheel and rail. The coupled mechanical–thermal behavior of wheel and rail materials under rolling contact is studied to determine the temperature rise due to the frictional heat. The wheel–rail frictional rolling contact problem is solved using the both hertz three–dimensional finite element (FE) method. The FE model considers the wheel tread–rail top contact with partial-slip and converts the frictional energy into the heat as an attempt to estimate the temperature rise. The assembly of wheel-rail geometry is created by CATIA V5R20 software. The finite element program ANSYS workbench is used to model the couple of thermos-mechanical rolling –sliding contact analysis and used to simulate the loading and boundary conditions of the wheel-rail rolling/sliding contact. When the couple of mechanical – thermal (maximum pressure and different heat flux) applied on the wheel – rail rolling/ sliding contact, it generates a maximum amount of heat and stress between rail and wheel. This cause plastic strain development and reduction of stress fatigue life for the increased value of loads that resulted from slippage as can note from analysis and simulation results. Rolling contact stress states and material response of wheel – rail under four traction coefficient and the same varying of sliding velocity were investigated. 3D coupled thermomechanical FE model were developed to analyze the temperature rise due to high applied load at contact and the thermal influence on residual stress-strain, wear and rail life.

Table of contents page

List of Table

List of Figure

ACRONYMS

β_w: Thermal Penetration Of Wheel

β_w: Thermal Penetration Of Rail

ε: Heat Partition Coefficient

μ_f: Kinetic or Static Coefficient

μ_r: Rolling Friction Coefficient

λ : Thermal Conductivity

ρ: Density Of The Material

a : Major Semi-Axis (Ellipse) Of Contact Patch

b: Minor Semi-Axis Of Contact Patch Ellipse

C : Specific Heat Capacity

Fn: Normal Force

F_t: Tangential Force

$Kair$ conductivity of air

K_1: Constants That Depend On The Material Properties Of Wheel

K_1: Constants That Depend On The Material Properties Of Rail

K_{22}: The Principal Transverse Radius Of Curvature Of The Wheel

K_{21}: The Principal Transverse Radius Of Curvature Of The Rail

K:	Thermal Diffusivity
Kv	air speed factor
L:	Thermal Penetration Depth
Nu	Nusselt number
m & n :	Hertz Coefficient
P:	Contact Pressure
$P_{e:}$	Pe'lcet Number
Po:	Maximum Pressure
$q_{w\ friction}$:	Frictional Heat Source
Re	Raynold number
r_w	Radius of wheel
S:	Longitudinal Creepage
UIC:	International Union Of Railway
V :	Forward velocity
v_{air}	kinematic viscosity
V_{iar}	Air speed
Vo:	Vehcle Velocity
Vr :	Rail Sliding Velocity
Vs:	Sliding Velocity
Vw:	Wheel Sliding Velocity

CHAPTER ONE

INTRODUCTION

1.1 BACKGROUND

The use of railway (railroad) tracks started some 200 years ago. These two centuries, and especially the recent years, saw dynamic advances in the different fields of railway engineering. From among the ordinary surface transportation forms, railway transportation is the safest and has the smallest energy and space demand, compared to its competitors. Thus it provides an economical solution in both freight and passenger transportation.

The railway network construction in Ethiopia was first started in October 1897 from Djibouti. In Ethiopia, The first rail transportation (train service) began on July 22, 1901, and operated between Djibouti and Douala, the first station on the Ethiopian side of the frontier at kilometer 106, a journey of 5 1/2 hours [1]. By 1915 the line reached Akaki, only 23 kilometers from the capital city, and two years later came all the way to Addis Ababa itself [2]. This marked the official commercial opening of the 784 km long railway although the Station of Addis Ababa was not inaugurated until 3 December 1929. For many years the railway operation was interrupted. Now the railway is currently being rebuilt and electrified by Chinese and Turkish companies. It is scheduled to be completed by September, 2015. And will be 756 km in length. The new railroad is expected to reduce the travel time from Addis Ababa to Djibouti by half to less than ten hours with a designated speed of 120 km/h [3]. Additionally, Addis Ababa light rail is under construction. It is constructed by china railway group limited. The Ethiopian railway corporation began construction of the 34.25 km double track electrified light rail transit project in December 2011[4]

The railway transport system is one of the most crucial transport systems in the world with higher speed and higher axle loads, higher reliability and safety, large carrying capacity (volume), lower life cycle cost (LLCC), satisfy environmental demands and higher availability and fewer disturbances comparing with roadway. Now days, there is high demand of railway transportation system in the world including Ethiopia for a long and medium distance transportation of passenger

and goods (freight). To satisfy such demands, it needs to have a railway transportation system with standard safety, comfort, speed, economy and reliability of the network. At the top of every system safety comes and has no compromise. Among many complex analyses of the railway network, this paper focuses on the effects of heat flux and pressure applied on wheel- rail during rolling/sliding contact . This study mainly concentrates on the effectiveness and side effects of varying sliding velocity and traction coefficient are considered. Modern railway vehicle cars alike are equipped with anti-block brake systems.

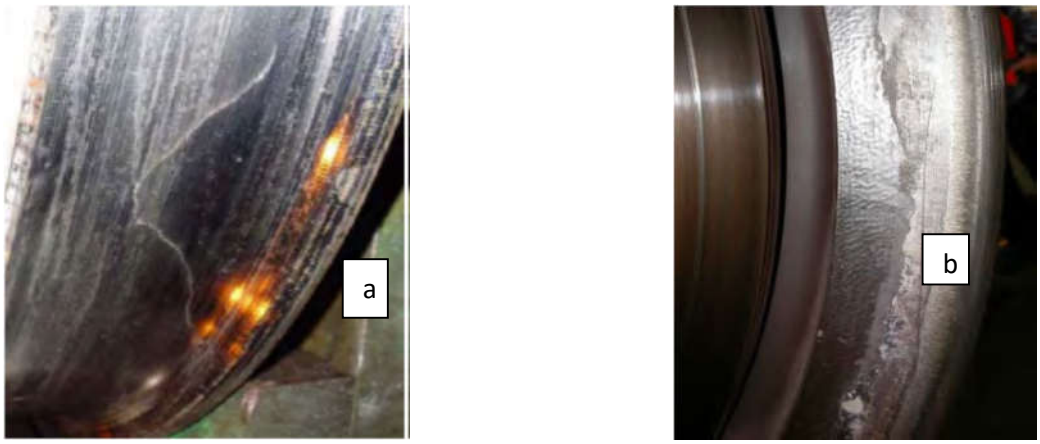

Figure 1 : Sub-surface fatigue crack (identified during wheel turning Figure 2b) Sub-surface fatigue crack (extending to back of wheel [5]

The contact surfaces of wheel and rail are subjected to high stress and high temperature generated by wheel-rail friction. The high temperatures of the surfaces due to wheel-rail friction occur instantaneously. Nevertheless, lower temperatures can lead to residual strain which assists to the appearance or the growth of micro cracks.

1.2 PROBLEM STATEMENT

Heat generation due to friction at the contact surfaces between wheel and rail is a common problem in railway engineering. Thermal damage caused by frictional heat of rolling-sliding contact is cause for failure forms of wheel and rail. This heat can raise the temperature of the tread

surface of the wheel above the allowable temperature. Due maximum heat generated it causes material phase change, deformation and formation of crack initiation and fatigue on wheel and rail material and also the increment of heat between rail and wheel was it reduced performance of train speed. The most significant one is loss of adhesion during attractive effort which causes significant heat generation at the contact of rail and wheels.

In the previous research, Mechanical load stress-strain analysis only was applied on wheel – rail contact. But mechanical load analysis only couldn't solved the problem of wheel –rail contact but also it is necessary to apply the thermal load. Some examples of using finite element analysis (FEA) for investigating the frictional heat generation and temperature rise in contact bodies were not considered during mechanical load stress- strain analysis. During rolling – sliding there were lack of equal distribution of thermal and stress distribution that causes fatigue on wheel- rail material contact. The damage of this wheel-rail contact was risk for derailments of wheel and also it imposes to high maintenance cost.

This research is proposed to address at least following questions:-

- What is the distribution of the contact pressure in the wheel–rail contact?
- What is the temperature distribution on and under the wheel tread/rail head during the first sliding/rolling?
- What will is the effect of temperature on wheel-rail material?
- What will are the effect of pressure on wheel-rail contact?

1.3 OBJECTIVE

1.3.1 General Objective

The general objective of this thesis is to analyze the effect of thermo–mechanical coupling on railway wheel-rail sliding-rolling contact using semi-analytical and finite element method.

1.3.2 Specific Objective

- ❖ Analysis of temperature and heat flux load acting at rail - wheel contact area.

- 3-D model of wheel-rail by using symmetry boundary condition.
- By using ANSYS software analyze the thermo – mechanical effect on wheel-rail during rolling –sliding contact.
- Modeling and analysis of combined thermal and mechanical loads.
- To predict the effects of this thermo- mechanical coupling on rail-wheel material.

1.4 Scope Of The Study

A railway car total axel load of 25kN used for this study which is the load applied on wheel will be 12.5kN. The thermo-mechanical wheel – rail contact assumed due to the mechanical and thermal loads. The analytical will analysis for elastic behavior of material properties and simulation is carried out for straight track and carried out for four traction of coefficient (0.3, 0.4, 0.5, and 0.58) and sliding velocity of (4, 8, 12, 16)condition. The vertical load and lateral load effect of the wheel are considered during the FEA.

1.5 Limitation Of The Study

Experimental testing equipment used for thermo-mechanical effect on wheel/rail material during sliding-rolling. Thus was helpful to compare the thermo– mechanical (semi-analytic FE result) with FE simulation. But due to lack full laboratories the study does not include experimental test. There are a lack of ultrasonic technique which used to determine the shape and size of the contact area.

1.6 Research Method

During my research to model and investigate the theoretical background of thermal wheel surface damage development. After the detailed analysis of the available methods, so to solve for the thermal and stress analysis of railway wheel-rail Rolling-sliding contact the following method are important.

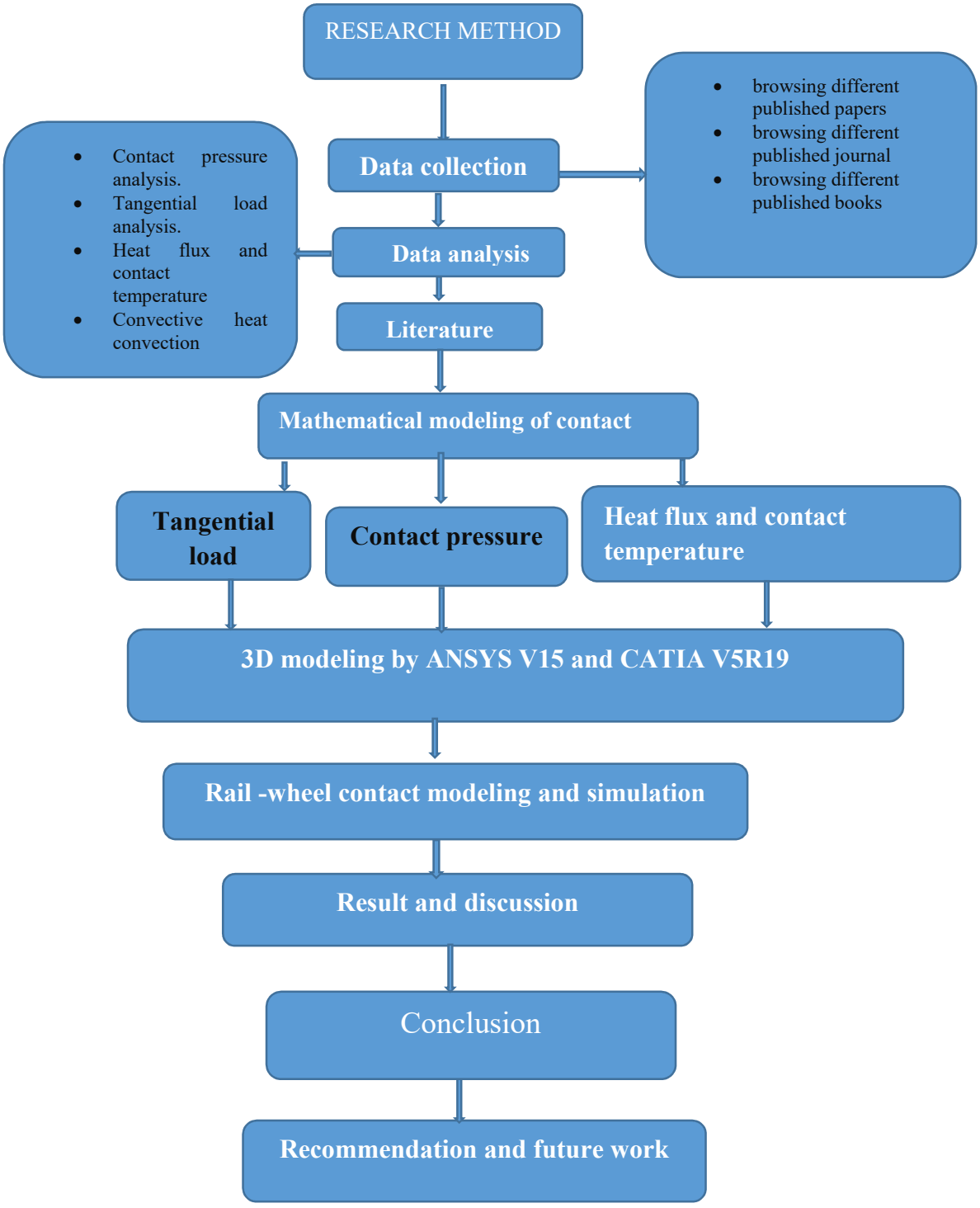

Figure 2 : Research method flow chart diagram

CHAPTER TWO

2.1 LITERATURE REVIEW

In the dissertation, [6] he studied the thermal and frictional state of railway wheel–rail contacts. In his goal, he was to study the thermal processes in the rolling-sliding contact between wheel and rail during intensive braking in the presence of a so-called WSP (Wheel Slide Protection System) anti-skid control system. As a result of the generated rolling contact during macroscopic sliding, micro-cracks may appear on the wheel tread and cause wheel failure. In his first method he used finite element model to analyze the wheel-rail normal contact. The shape and the dimensions of the contact patch and the maximum contact pressure have been evaluated. Using the basis model, the starting process of the wheel from stationary position with an average μ=0.15 frictional coefficient was simulated which is the inverse of what happens during the braking of a rotating wheel. In the next phase of his study, he narrowed down the focus to a specific part of the investigated region and used the results of the earlier study to create another FE model to investigate the thermal processes of a specific wheel–rail contact during intensive braking, studying the wheel and rail surface behavior assuming a slip of 15 %.

As shown by the results, the sudden temperature rise results in stresses exceeding the yield strength on the tread surface and 0.2-0.5 mm under the surface (i.e. the initial compressive stress changes to tensile stress), and these stresses and their cyclic nature may promote the formation and appearance of micro-cracks on and under the wheel tread surface.

As [7] the profile of the wheel is conical with 1/20 therefore the more affected area of the wheel is the area with the lower radius which is tip of the wheel. But the maximum temperature rise occurs at the middle of the contact between wheel and the tread block due the critical contact area is on center point of the tread of the brake shoe. Since the maximum energy generated by the train is at the station on the north-south line at the station NS22 the maximum temperature rise also occurs at this station. The initial temperature of the wheel and the surrounding (environmental temperature) is 25.5℃. When coming from station NS21 the wheel cools down to557.58℃ and 366.88 for the wheel contact of 30 and 45℃ . The temperature of the surrounding is still 25.5°C.

In case of braking the train at NS22 station the highest temperatures reach up to 1001.9°C for the contact angle 30°and 662.8 for 45°. This temperature is reached at a time period of 16 s. The area directly beneath the braking pad carries the main burden. This is also the place where the highest temperatures are achieved. The figures show how the temperatures toward the wheel rim fall. This information is needed to determine the influence of the heat flux on the wheel tread. As in the case of temperature rise the maximum heat flux occurs at the tread of the wheel due the contact between wheels and tread block. The difference is the maximum heat flux distribution occurs at the end point of the wheel due to its conical with lower diameter of the wheel tread at this point. Since the heat flux is directly related to the temperature the maximum heat flux occurs at the station on the north-south line at the station NS22. There for from the analysis the maximum het flux on the wheel tread is about $2.1077*10^6 W/m_2$ for θ=30°and for θ=45° reaches about $1.6504*10^6 W/m^2$.

The body temperature raised as a result of braking is imported to the structural transient analysis for further use to determine the stress and deformation. Different result of temperature for both cases (i.e. 30° and 45° angle) result in different stress and deformation in addition with the loads on the wheel due to braking and weight transfer of the vehicle which is constant throughout the motion of the train.

This maximum temperature rose when the train stopped is used together with other mechanical loads calculated in chapter three to determine the maximum equivalent (Von messes) stress imposed on the wheel. From the output result of the analysis the minimum equivalent (Von messes when the train starts braking is $2.548*10^7 N/m_2$ and the maximum equivalent (Von messes) stress induced on the wheel is about $2.6028*10^9 N/m_2$ θ=30°and $1.5044*10_6$ and $1.6675*10_9$ for 30° respectively. When the railway train starts moving from rest the environmental or ambient temperature of the train component is the same as the environmental temperature. As the train starts moving the kinetic energy of the train increases and gets maximum at the maximum speed. As the train moves up the grade of the potential energy decreases and vice versa while moving up the gradient. Since the total energy reaches maximum at maximum speed, its temperature reaches some value because there is no heat dissipation from the train but this temperature is the maximum temperature while the train is moving. When the driver starts to brake the train the,

heat dissipation from the train to the environment stars to rise and reaches maximum when the train fully stops.

A coupling thermo-mechanical model of wheel/rail in rolling-sliding contact is put forward using finite element method. The normal contact pressure is idealized as the Hertzian distribution, and the tangential force presented by Carter is used. In order to obtain thermal-elastic stress, the thermal-elastic plane stress problem is transformed to an elastic plane stress problem with equivalent fictitious thermal body force and fictitious boundary distributed force. The temperature rise and thermal- elastic stress of wheel and rail in rolling-sliding are analyzed. The non-steady state heat transfer between the contact surfaces of wheel and rail, heat-convection and radiation between the wheel/rail and the ambient are taken into consideration. The influences of the wheel rolling speed and wear rate on friction temperature and thermal-elastic stress are investigated. The results show the following: ①For rolling-sliding case, the thermal stress in the thin layer near the contact patch due to the friction temperature rise is severe. The higher rolling speed leads to the lower friction temperature rise and thermal stress in the wheel; ②For sliding case, the friction temperature and thermal stress of the wheel rise quickly in the initial sliding stage, and then get into a steady state gradually. The expansion of the contact patch, due to material wear, can affect the friction temperature rise and the thermal stress during wear process. The higher wear rate generates lower stress. The results can help understand the influence of friction temperature and thermal-elastic stress on wheel and rail damage [8].

Slippage is great problem for locomotive which do not have slip control. In order to address the problem research have tried to model and analysis its effect starting early times. Some of them are discussed as follow. Temperature rise due to slip between wheel and rail-an analytical solution for hertzian contact presented. Most of the researches are only concerned only thermal or on stress analysis separately. In each study only one of the method was applied, which not satisfactory for accuracy of the analysis [9].

But in present thesis I will analysis those problems caused by coupling thermal and mechanical analysis; at the wheel – rail rolling –sliding contact. During the couple of thermal and mechanical, the material of the wheel and the rail are considered as the same. These fields also provide opportunities for improve the accuracy of the solution by varying of both sliding velocity and

traction coefficient. The coupling of thermal and mechanical will be depend on the plastic – elastic FEM analysis. Since it is difficult to measure the temperature and pressure during vehicle rolling/sliding, so, it is important to approximate the influence of both thermal – mechanical coupling by using analytical and ANSYS V15 software which are used to strength the result I will obtain.

CHAPTER THREE

3.1 THEORETICAL BACK GROUND OF WHEEL RAIL CONTACT

3.1.1 Wheel/Rail Contact Stress

Assessment of contact stresses at the wheel–rail interface is one of the most important aspects of railway research, considering the many phenomena involved (wear, adhesion, surface fatigue damage, etc.). Due to elastic properties of the materials this point will deform to a contact area. The deformation that occurs will produce high tensile and compressive stresses in the materials. Even if, a singular loading does not produce a failure, it can lead to future fatigue or surface damage. The maximum pressure within the contact area occurs as a compression in the center. The total stresses developed in the rail are the sum of the stresses at the wheel/rail contact (named as Hertz stresses).

3.1.2 Characteristics of the Wheel-Rail Contact

The wheel-rail profiles are always designed to follow the standards which depend on the operational conditions in each country. The main sections of a wheel profile include flange, tread and chamfer as plotted in Figure below. The wheel profiles are normally inclined at a small angle.

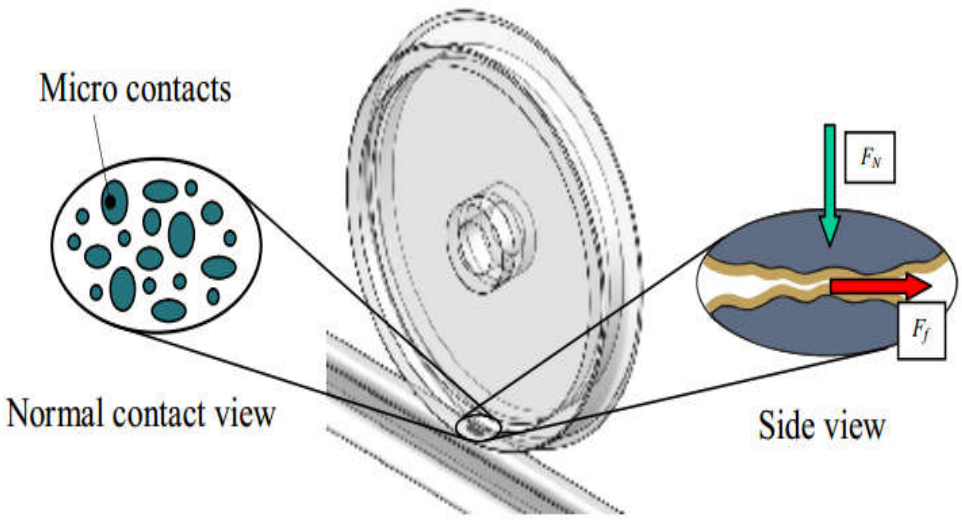

Figure 3: Wheel-rail contact and friction

The contact can be approximated by an elliptical Hertzian contact and will be used in this thesis. At microscopic scale, the two contacting bodies (wheel running band and top of the rail) are rough and contact take place on roughness level. As stated earlier, the wheel – rail contact is considered to be "lubricated" for the low friction case so the friction force is to be calculated by using adequate shear models for the interfacial layer present in the micro contacts and remaining macro contact. Wheel - rail contacts are sliding/rolling contacts, meaning that the peripheral velocity of the wheel is comparable within limits with the total velocity of the train [10].

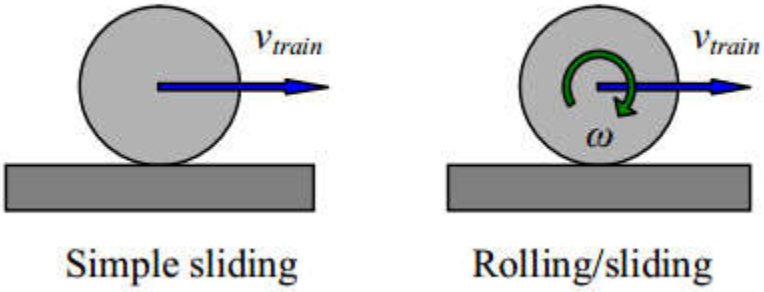

Figure 4 : Rolling/sliding wheel - rail contact.

From pure rolling ($v_{train} = v_{wheel}$) to simple sliding ($v_{wheel} = 0$ and $v_{train} \neq 0$) the coefficient of friction between the wheel and the rail would increase from zero (pure rolling) up to a friction value caused by shearing corresponding to the considered lubrication situation. Such variation represents the so-called traction curve. Other dependency of the coefficient of friction is given by varying the rolling velocity between the wheel and the rail. With increasing the velocity, the coefficient of friction decreases due to lift-off of the wheel because of pressure built up in the interfacial layer. This variation, i.e. coefficient of friction as a function of sum velocity, is the so-called Stribeck curve. Apart from the theoretical modelling of the friction between wheel and rail, equally substantial insight is given by directly measuring the friction between a contacting probe and the counterpart (wheel and top of rail). Such equipment is of use to validate a friction model.

3.1.3 Rolling and Sliding

Rolling is defined as a relative angular velocity between the two bodies in contact about an axis parallel to their common tangent plane. The Percentage of sliding can also be involved, and introduce differences in rotational speeds of the contacting bodies. This phenomenon is called (partial) slip. If no torque is applied on the rolling element, the contact situation is called free rolling. Apart from slip on a micro-scale, free rolling contacts will involve almost no macro-slip. The situation in which one of the rolling elements is driven is called tractive rolling. Tractive rolling may result in fairly large amounts of slip. So the increase in the sliding percentage or slip of the motion is related to the change of the contact from an ideal rolling situation to a state in which a percentage of tangential components are introduced. Well-designed rolling contacts only fail after many cyclically loaded contacts. However, in the initial stages localized plastic deformation may occur in rolling contacts. Running-in is an example where initial small scale plastic deformation of the asperities is having the effect of generating more favorable running surfaces. If certain conditions are satisfied, initial plastic deformation in rolling contacts may result in an elastic steady state situation after a certain number of rotation.

3.1.4 Rolling Contact Mechanics

In rail vehicles, the contact forces that roll and carry the load of train happen in the tiny contact area roughly, where steel wheel meets steel rail [28]. As a result, the wheel rail contact is extremely complex. A broad interdisciplinary research is needed to understand, model and optimize the contact mechanics and dynamics problem. The contact stress distribution prediction is the key to many wheel-rail related problems such as wear, rolling contact fatigue (RCF), plastic deformation, etc. As wheel and rail come into contact due to external force, deformations of microscopic asperities happen at the interface. Due to relative motion between the bodies, contact forces between two bodies appear. The tangential force at the contact is known as adhesion force or creep force. Adhesion or creep is different from (sliding) friction (Figure 5). Figure 5-Left shows a block sliding on a stationary surface with a velocity of v_s. the free-body diagram of the block includes a normal force (F_n) usually is the weight of the block) and horizontal friction force (F_f). The horizontal force is equal to kinetic friction force, which is generally lower than static friction force.

The static friction force is the force required to initiate sliding of the block against the surface, whereas the kinetic friction force is the force required to maintain sliding. The ratio between the static or kinetic friction force and the normal force is called the static or kinetic.

$$\mu_f = (\frac{F_f}{FN}) \quad (1)$$

Figure 5-Right shows a wheel or roller rolling along a surface/rail with an angular velocity of ω and a forward velocity of V, like a locomotive wheel rolling on a rail. The wheel is subjected to a driving torque (T) and normal force (F_n). The torque maintains the angular velocity of the wheel and also causes a reactive tangential force (F_t). The tangential force is the creep/adhesion force at the interface and propels the wheel along the rail. The ratio between the tangential (adhesion) force and normal force is called the adhesion (rolling friction) coefficient:

$$\mu_r = (\frac{F_t}{FN}) \quad (2)$$

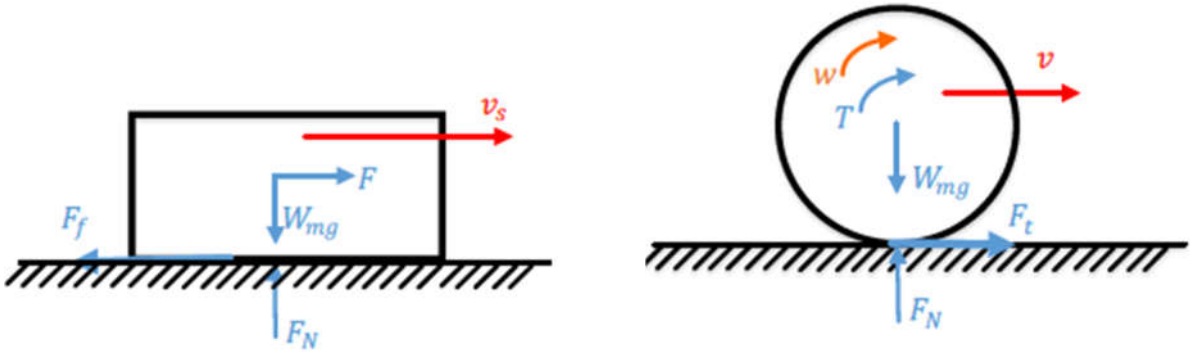

Figure 5 : Schematic drawing of pure sliding contact (left) and rolling contact (right) [11]

To maintain a constant velocity of the wheel or accelerating the wheel, the circumferential velocity of the wheel at the interface (wR) for a driven wheel will always be greater than its forward velocity (v).

3.1.6 Heat Induced By Frictional Rolling

Friction conditions can seriously affect the rail life, for instance heat generation at the contact zone [12]. The wheel-rail contact zone can be split into stick and slip regions due to frictional

rolling contact. If the traction or braking forces exceed the available adhesion, gross slipping happens which extensively generates heat at the contact spot.

3.1.7 Contact Temperature

3.1.7.1 Frictional Heating.

The power dissipation due to tangential stress and sliding velocity between wheel and rail results in contact temperatures that can exceed 200 ℃ under normal operating conditions. They are confined to a very thin surface layer. The thermal penetration depth depends on the non-dimensional Pe´clet number with the semi-axis length a, the speed v of the moving heat source and the thermal diffusivity [13].

$$\delta = \frac{a}{\sqrt{L}} \tag{3}$$

$$L = \frac{av}{2k} \tag{4}$$

$$k = \frac{\lambda}{\rho c} \tag{5}$$

Where , λ =thermal conductivity

ρ = density of material

c = specific heat capacity

High contact temperatures occur at high values of the sliding velocity vs. In this case, elastic deformations of the wheel and rail can be neglected and the distribution of frictional heating for Hertzian contact is [14].

$$q_{friction} = \frac{\mu |v_s| \, p_z(z)}{\sqrt{1-\xi^2}} \tag{6}$$

It is generally assumed that the dissipated frictional power is completely transformed into heat. The heat flows into the material of the wheel and rail. With equal thermal properties of the wheel and rail, the heat partitioning factor depends only slightly on the different velocities of wheel, different traction coefficient and rail with respect to the area of contact. Either a transient

calculation with very small time increments or the concept of ALE (Arbitrary Eulerian–Lagrangian) relative hardening kinematics, would be required for the adequate treatment of the problem. Additionally, the discretization should be extremely fine in the component direction due to the very small thermal fatigue.

3.1.8 Thermal Loads

To obtain temperature rise due to braking, it is assumed that the entire frictional energy between wheel-blocks (brake power) converts to heat and this heat, distributes among rail, wheel and brake blocks [15]. Hence, for determining temperature rise of these components, it is necessary to know the heat partition factor of rail - wheel and wheel-block contact regions. At the beginning of wheel sliding on the rail, heat partition factor between rail and wheel (σ) is equal to 0.5; this is due to considering the same physical and thermal properties for the wheel and the rail. By increasing the slip time, this factor reduces, which means that the most of heat generated due to slip is transferred to rail. The reason for this reduction can be based on the fact that during rotation of the wheel on the rail, a new rail surface is always subjected to the high temperature wheel surface; therefore, the rail surface should absorb this generated heat until attained to the wheel temperature. As mentioned, in the beginning of sliding, this parameter is equal to 0.5 (transient state) and after some times (less than 1 s) it reaches a constant value (steady state). At interval of these two states, varies as a function of time.

3.1.9 Thermal Stresses

The contact temperature gives rise to severe thermal stresses at the surfaces of wheel and rail. An accurate analysis of this problem would only be possible with a finite element model. But since the large changes in temperature are confined to a very thin surface layer, we can assume that the expansion of the surface in the x- and y-directions is zero while the expansion in the z-direction is possible without restriction [16]. Thus the pure thermal loading results in a state of plane.

$\in_x = 0$, $\in_y = 0$ and $\sigma_z = 0$, then the thermal stress are

$$\sigma_x = \sigma_y = \frac{-\alpha \Delta \boldsymbol{T}}{1-\upsilon} \tag{7}$$

With the young's modulus E, the thermal expansion coefficient α and poison's ratio υ.

3.1.10 Couple Thermal and Mechanical Stresses

The method of thermo-mechanical analysis for both wheels and rail does thermal analysis on the whole model (consisting of wheel, rail and blocks) and yields the temperature rise; then in the second stage, these obtained temperatures are applied to the wheel model as initial thermal loads and by introducing a thermal expansion factor of components, thermal stresses due to these thermal loads can be calculated.

3.1.11 Effect of Coupled Forces

The wheels, which are acted upon by the mechanical forces, also experience thermal loads during service, due to braking [17]. The effect of these coupled stresses will be analyze in order to understand the stress levels at various points on the wheel. The aim of this work also includes prediction of temperature and thermal stress distributions on the wheel due to intensive braking. A sequentially coupled analysis have perform for this problem, since the deformation field of the wheel or rail depends on the temperature field. This temperature field can be find without the knowledge of the deformation response. Hence, the heat transfer analysis is performed first and then followed by the elastic-plastic analysis. The respective nodal temperatures as derive from the heat transfer analysis are also taken into account along with the mechanical load.

CHAPTER FOUR

4.1 MODELING OF COUPLE THERMO- MECHANICAL OF WHEEL-RAIL ROLLIG-SLIDING CONTACT

This model will be develop for the thermos - mechanical solution of the frictional rolling/sliding contact [18]. The model is further advance in the present research to deal with the thermo-mechanical problem. It simulates the wheel–rail contact with frictional heat generation during rolling and sliding. The material thermal structural response is simulated using finite element method and Hertzian pressure distribution which capable of solving for the transient temperature under thermal/mechanical boundary conditions. A coupled of mechanical– thermal approach is used to estimate the flash– temperature at the wheel–rail interface.

To perform the coupled analysis, the heat flux is firstly computed by the frictional contact (mechanical solver). Then, this is given as the input of thermal analysis for determining material thermal response. This leads to the distributions of stresses as well as temperature along wheel – rail surface. Work done by friction can be transformed into fatigue life, shear stress, stress life and heat. By selecting appropriate time steps for modeling, the mechanical and thermal solvers are connected in an iterative solution scheme.

Using this coupled analysis the following advantages can specifically be considered:

- In the coupled analysis, material properties can be assumed to be temperature dependent.
- The geometries of the materials and the transient temperatures are spontaneously updated during the coupled simulation. Therefore, the effects of mechanical load and temperatures are interactively considered. This makes the model more accurate using a thermal and mechanical analysis under the presence of the heat flux and pressure.
- The stresses are dependent on the temperature distribution in the frictional rolling contact. The coupled approach gives more realistic stress responses since the mechanical and thermal solutions are obtained simultaneously during the numerical simulation.

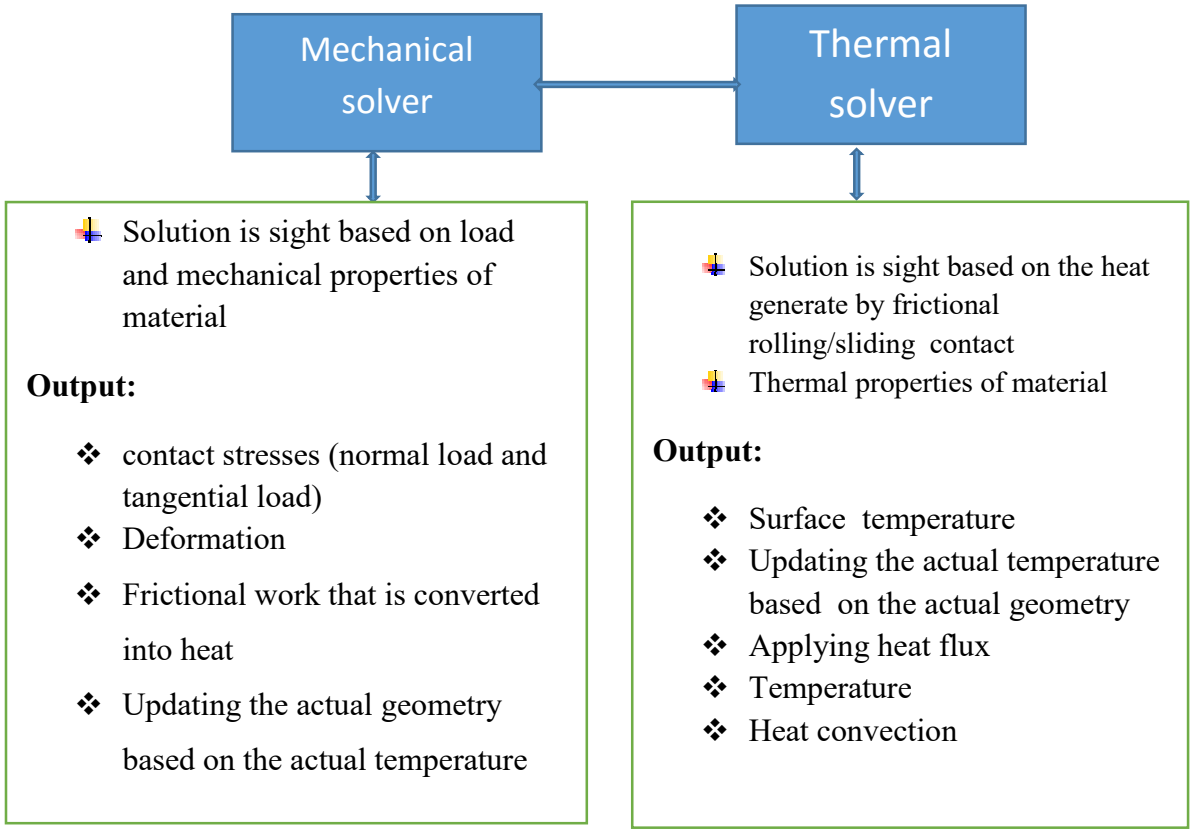

Figure 6 : The coupled mechanical-thermal analysis with the proposed FE tool

4.1.3 Model of Temperature Wheel-Rail Contact

Using FEM, a numerical model is developed in a more realistic way. A 3D transient FE model will be built to examine the mechanical-thermal coupling behavior of the contact bodies with arbitrary geometries under frictional rolling contact. Among the above-mentioned assumptions which limit the applicability of the analytical methods, finite element method will use in the present research. However, the temperature solution is sight for the 3D contact problem with partial slip, by using a transient time integration scheme. The heat flux is generated in the slip region. Rolling contact with frictional heat generation is simulated with the wheel running with a constant speed on the rail [19].

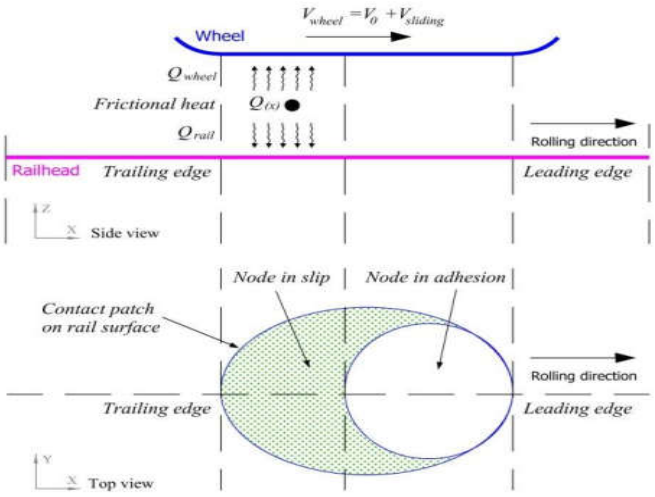

Figure 7 : Calculation of the temperature in partial-slip [14]

4.1.4 Boundary Condition for the wheel- rail Model

For modeling the wheel and rail, profile of railway car is used which have wheel diameter of 660 mm which is amongst the most common wheels in the ERC was applied [20]. UIC50 rail is modeled with wheel (UIC 812-3/EN S1002 which are similar to Addis Ababa LRT specification and the sample length of 600 mm considered. In this study an axle load of 25kN which is F = 12.5kN vertical loads on a wheel of freight car running 19.4 m/s (70km/hr.) on the straight track is considered. The 3D model of the 660mm diameter wheel and 600 mm long rail is model using CATIA R20 V5 for simulation of rail head and wheel tread contact.

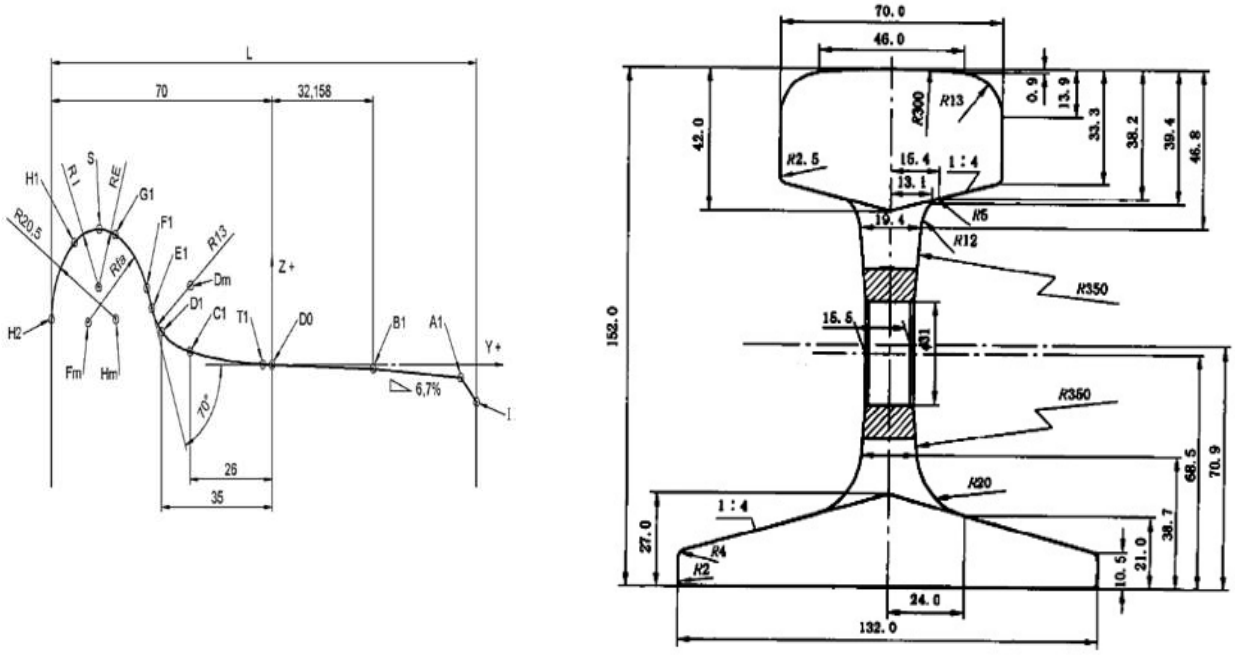

Figure 8 : UIC-50 Rail and wheel profiles models [26][19]

4.1.5 3D Modeling of Wheel –Rail Contact

Contact zone with surface temperature is created by means of sub modeling on the wheel as well as on rail contact point in ANSYS. The contact stiffness is selected to be augmented Lagrange contact stiffness of solid to solid surface contact method. It is recommended for general frictional contact in large-deformation problems. Augmented Lagrange formulation method is very similar to that of penalty method without rapped effected except that it reduces sensitivity to contact stiffness. Beside the contact is modeled to have Symmetric behavior. This means that the Contact surfaces are constrained from penetrating the Target surfaces and the Contact surfaces are constrained from penetrating the Contact surfaces area. The modeled geometry are analyzed without large gap of penetration.

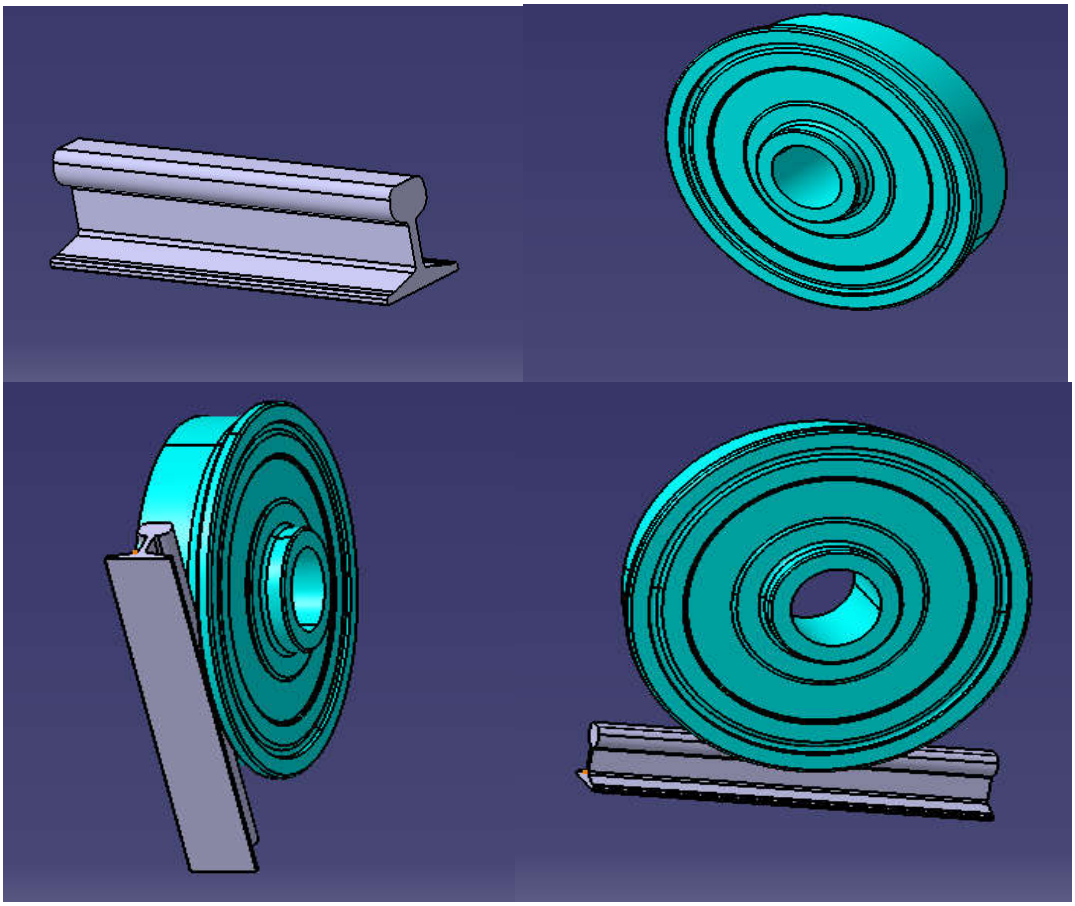

Figure 9 : Rail-wheel assembly modes on CATIA rail head to wheel tread contact

4.1.6 Principal and Shear Stresses

According to Hertz contact theory, on the point of contact the maximum principal stress is perpendicular to the plane of contact point, which is on the line of applied load. The applied load can be either compressive or tensile. The remaining principal stresses are equal. The yield criteria can be expressed in terms of the stress state, strain state, and thermal strain quantity. The common yield, known as the von Misses yield criterion predicts that yielding will occur whenever the distortion energy in a unit volume equals the distortion energy in the same volume when uniaxial stressed to the yield strength. From this theory, a scalar invariant (Von Misses equivalent stress) is derived as.

$$\sigma_e = \sqrt{0.5\,[(\sigma_1 - \sigma_2)^2 + (\sigma_2 - \sigma_3)^2 + (\sigma_2 - \sigma_3)^2 + (\sigma_3 - \sigma_1)^2} \quad (8)$$

When von Mises equivalent stress exceeds the uniaxial material yield strength, general yielding will occur in this study von misses stress yield criteria is implement for stress analysis.

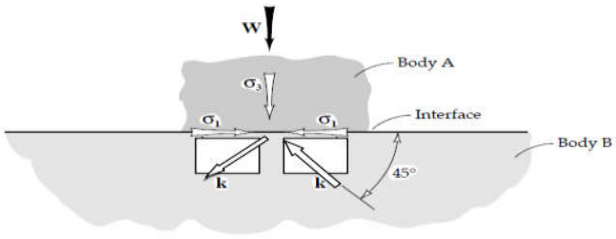

Figure 10 : Stress status in point contact; σ1, and σ 3 are the principal stresses, and k is the shear yield stress of the material.

4.1.7 Elastic limit

Yielding begins when the equivalent stress is equal to the yield limit σ_y. Here, we use the v. Mises yield criterion with the equivalent stress for a state of plane strain.

$$\sigma_{vm} = \sigma_y$$

$$\sigma_{vm} = \sqrt{(\sigma_x - \sigma_y)^2 - (\sigma_y - \sigma_z)^2 - (\sigma_z - \sigma_x)^2 - 6\tau xy} \quad (9)$$

In simple shear, the yield stress is $\sigma_y = \sqrt{3k}$. Since all components of mechanical and thermal stresses are proportional to p_0, the yield criterion can be used to calculate the maximum Hertz pressure p_0 called the elastic limit at which yielding begins. The stresses due to normal loading are equal in the wheel and the rail. For Hertz contact with full sliding, only the sign of the stresses due to tangential loading depends on the direction of the tangential force acting on the wheel and rail. Without thermal stresses, the distribution of the equivalent stress in the wheel and the rail is equal, but with reverse orientation. If the wheel and the rail are initially at the ambient temperature, the thermal stresses due to frictional heating are equal in both of them. But the distribution of equivalent stress is no longer the same in all cases because of the combined mechanical and thermal stresses.

CHAPTER FIVE

5.1 ANALYSIS OF COUPLE THERMO- MECHANICAL OF WHEEL-RAIL ROLLIG-SLIDING CONTACT

When a wheel and a rail get into contact under the action of the static wheel load, the contact area and the pressure distribution are usually determined by using the Hertz theory. Due to the complexity of the coupled mechanical–thermal behavior, numerical approaches will use for more frequently are some examples of using finite element analysis (FEA) for investigating the frictional heat generation and temperature rise in contact bodies. Besides the studies on thermal behavior of the frictional contact, extensive research has also to be carry out on mechanical aspects of the wheel–rail contact.

Using FE analysis, some studies will be investigate the coupled effects of the mechanical and thermal aspects. Although the numerical model of benefits from a 3D FE modelling, the thermal calculation is performed separately from the mechanical simulation (uncoupled analysis). The model uses a transient explicit solver and it is capable of estimating temperature rise in wheel-rail materials. In the mechanical part, the 3D transient FE model is able to solve both the normal and the tangential contact problems simultaneously for arbitrary wheel-rail geometries. In the thermal part, a heat flux analysis is used which is coupled with the mechanical solver.

In railway engineering, the wheel-rail contact patch becomes a slim elliptical shape in the lateral direction after a long-term wear.

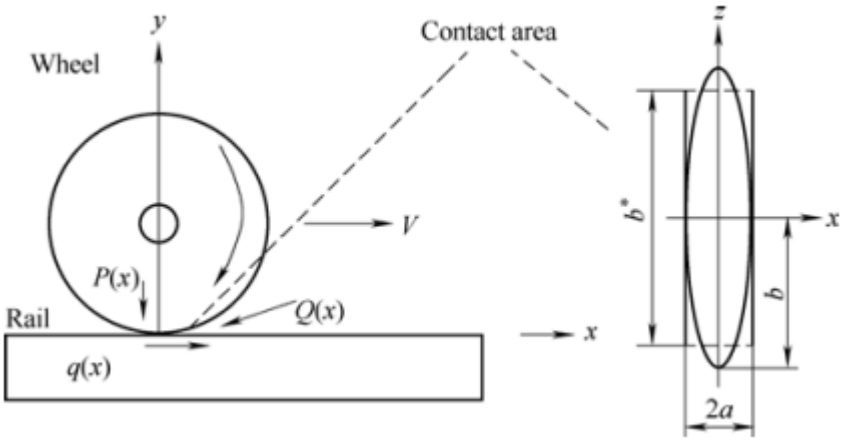

Figure 11 : Wheel-rail in sliding contact area [12]

5.1.2 MATHEMATICAL MODEL FOR WHEEL-RAIL CONTACT

First, According to Yan, if two elastic nonconforming bodies are pressed together then the contact area assumes elliptical shape with a semi major axis 'a' and a semi minor axis 'b'.

The distribution of the contact pressure in this elliptical area as shown in Fig 12 represents a semi-ellipsoid, expressed as [21]:

$$P = Po\left(1 - \frac{x2}{a^2} - \frac{z^2}{b^2}\right) \tag{10}$$

$$P_O = \frac{3W}{2\pi ab} \tag{11}$$

Where is the maximum contact pressure, *P* is the total normal contact force. *a* and *b* are the semi-axes of the contact ellipse.

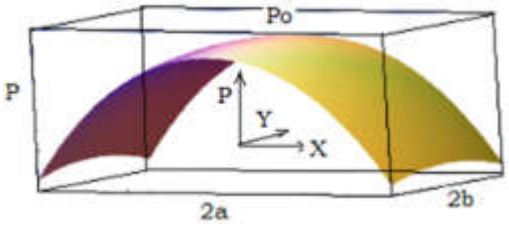

Figure 12 : Pressure distribution across elliptic area [12]

The method assumes the contact surfaces to be smooth, so they can be described by a second-degree polynomial

$$Z_1 = A_1x^2 + A_2xy + A_3y^2 \quad (12)$$

$$Z2 = B_1x^2 + B_2xy + B_3y^2 \quad (13)$$

Where *x* and *z* are the local coordinates in the longitudinal and lateral directions, respectively.

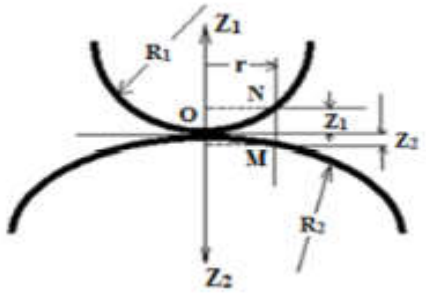

Figure 13 : General Profiles of two contacting bodies [12]

The contact plane is held immovable during compression. Any two points of the contacting bodies on the axes Z1 and Z2 at large distances from O will approach each other differing by a certain amount α, and the distance between two points such as M and N will diminish by α-(w1+w2).

From geometrical consideration it can be written as

$$w_1 + w_2 = \alpha - (Z1 + Z2) \quad (14)$$

Where, w1 and w2 denote the displacement of a point due to the local deformation in the Z direction respectively.

Using Boussinesq's solution for a semi-infinite body subjected to a concentrated normal force at the boundary surface displacement w1 and w2 [22] is given by:

$$\omega_1 = k_1 \iint P d\Psi \, ds \quad (15)$$

$$\omega_2 = k_2 \iint P d\Psi \, ds \quad (16)$$

Where K1 and K2 are constants given by:

$$k_1 = \frac{1-\mu 1^2}{\pi E1} \quad (17)$$

$$K2 = \frac{1-\mu 2^2}{\pi E2}, \tag{18}$$

And, μ & E also are elastic constants. Substitution of Eqn. above pro

$$(K_1 + K_2) \iint \frac{P\, dA}{\gamma} = \alpha - Ax^2 - By^2 \tag{19}$$

$$P_O = \frac{3P}{2\pi ab} \frac{3\pi P}{4} \tag{20}$$

$$a = m \left[\frac{3\pi P}{4} \frac{(K1 + K2)}{(A+B)}\right]^{1/3} \tag{21}$$

$$b = n \left[\frac{3\pi P}{4} \frac{(K1 + K2)}{(A+B)}\right]^{1/3} \tag{22}$$

The calculation of the contact areas requires knowledge of some geometric constants used in the above formulation. With respect to wheel-rail configuration, the following curvature combinations are related as:

$$A+B = \frac{1}{2}\left(\frac{1}{R_{11}} + \frac{1}{R_{12}} + \frac{1}{R_{22}} + \frac{1}{R_{21}}\right) \tag{23}$$

$$A+B = \frac{1}{2}\left(\frac{1}{R_{11}} + \frac{1}{R_{12}} + \frac{1}{R_{22}} + \frac{1}{R_{21}}\right) \tag{24}$$

$$B-A = \frac{1}{2}\left[\left(\frac{1}{R_{11}} - \frac{1}{R_{12}}\right)^2 + \left(\frac{1}{R_{22}} - \frac{1}{R_{21}}\right)^2 + 2\left(\frac{1}{R_{11}} - \frac{1}{R_{12}}\right)\left(\frac{1}{R_{22}} - \frac{1}{R_{21}}\right) cos2\Psi\right]^{1/2} \tag{25}$$

Where A and B are positive constants. R11, R12, R21 and R22 are defined as the principal relative radii of curvature, represented pictorially in the Fig. 14

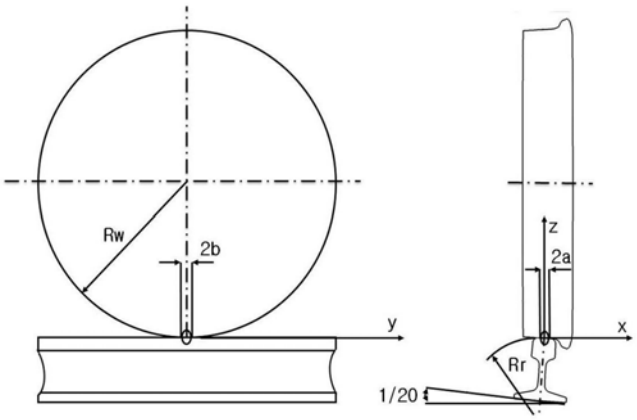

Figure 14 : Wheel-Rail Configuration showing different principal relative radii of curvature [24]

Where,

R11: The rolling radius of curvature of the wheel.

R12: The radius of the wheel profile, which goes to infinity for a conical wheel.

R21: The radius of the runway which is infinity in this case

R22: The radius of curvature of the rail in the plane of cross section.

The ellipticity parameter ($\frac{a}{b}$)is related to geometrical parameter ($\frac{A}{B}$)by means of the coefficients 'm' and 'n'. From the notation, cos θ ($\frac{B-A}{B+A}$) the values of m and n for various values of θ are will be calculate by:

$$n = 3E\text{-}0.5\theta 2 + 0.0045\theta + 0.334 \quad (26)$$

$$m = 62.19\theta^{-0.91} \quad (27)$$

The principal stresses at the Centre of the surface of contact [23] are calculated as:

$$\sigma_1 = -2\mu P_o(1-2\mu)P_o\frac{b}{a+b} \quad (28)$$

$$\sigma_2 = -2\mu P_o(1-2\mu)P_o\frac{a}{a+b} \quad (29)$$

$$\sigma_3 = -P_o \quad (30)$$

The material model is linear-elastic and there is friction between the contacting surfaces. The contact total load is taken as 25kN. Material data $E_1 = E_2$ =210 GPA, μ =0.3, are used for the pair of contacting bodies, R11=330 mm, R12= ∞ mm, R21=∞, R22=300 mm. to calculate the value by using equation of [15-30]:

$$k_1 = \frac{1-\upsilon_1}{\pi E1} = \frac{1-0.3^2}{\pi 210e^9\ N/m} = 1.38e^{-12}N/m$$

$$K2 = \frac{1-\mu 2^2}{\pi E2} = \frac{1-0.3^2}{\pi 210e^9 N/m} = 1.38e^{-12}N/m$$

$$A+B = \frac{1}{2}\left(\frac{1}{330mm} + \frac{1}{\infty} + \frac{1}{\infty} + \frac{1}{300mm}\right)$$

$$= 0.0032/\text{mm}$$

$$B\text{-}A = \frac{1}{2}\left[\left(\frac{1}{R_{11}} - \frac{1}{R_{12}}\right)^2 + \left(\frac{1}{R_{22}} - \frac{1}{R_{21}}\right)^2 + 2\left(\frac{1}{R_{11}} - \frac{1}{R_{12}}\right)\left(\frac{1}{R_{22}} - \frac{1}{R_{21}}\right)cos2\Psi\right]^{1/2}$$

For this case the angle ψ between the radius of the wheel and rail is $\Psi/2$, then

$$B\text{-}A = \frac{1}{2}\left[\left(\frac{1}{330} - \frac{1}{\infty}\right)^2 + \left(\frac{1}{300} - \frac{1}{\infty}\right)^2 + 2\left(\frac{1}{330} - \frac{1}{\infty}\right)\left(\frac{1}{300} - \frac{1}{\infty}\right)cos2(\pi/2\right]^{1/2} = 0.00225$$

Then to calculate the value of θ along wheel sliding rail

$$\text{Cos}\ \theta = \left(\frac{B-A}{B+A}\right) \tag{31}$$

$$\text{Cos}\ \theta = \left(\frac{0.00225}{0.0032} =\right) = 0.703$$

$$\theta = cos^{-1}(0.168) = 50°$$

After calculation we have the following values for A+B, A-B and θ, 0.0032/mm, 0.00225 and θ= 50° respectively. This angle used for interpolation calculation of m and n. By using the following Table (the Hertz coefficient), linear interpolation method and the intermediate values of m and n of the rail are calculated using regression given by:

Table 3.4 The Hertz coefficient m and n [14]

θ (deg)	m	n	θ (deg)	m	n	θ (deg)	m	n
0.5	61.400	0.1018	10.0	7.860	0.2850	60.0	1.486	0.7170
1.0	36.890	0.1314	20.0	6.604	0.3112	65.0	1.378	0.7590
1.5	27.480	0.1522	30.0	3.813	0.4123	70.0	1.284	0.8020
2.0	22.260	0.1691	35.0	2.731	0.4930	75.0	1.202	0.8460
3.0	16.500	0.1964	40.0	2.397	0.5300	80.0	1.128	0.8930
4.0	13.310	0.2188	45.0	2.136	0.5670	85.0	1.061	0.9440
6.0	9.790	0.2552	50.0	1.926	0.6040	90.0	1.000	1.0000
8.0	7.860	0.285	55.0	1.611	0.6780			

From the above Table to calculate to calculate the value of a & b [24] when $\theta = 50°$, m = 1.926 and n = 0.6040

$$a = m\sqrt[3]{3\pi W(k_1 + k_2)/4(A + B)} \quad (32)$$

$$a = 1.926\sqrt[3]{\frac{3\pi 12500(1.38e^{-12} + 1.385e^{-12})}{4\times 3.2/m}} = a = 5.65mm$$

$$b = n\sqrt[3]{3\pi W(k_1 + k_2)/4(A + B)} \quad (33)$$

$$b = 0.6040\sqrt[3]{\frac{3\pi * 12500 * (1.38e^{-12} + 1.38e^{-12})}{4\times 3.22/m}} = b = 1.77mm$$

Under the total vertical load of 25000 N of 2 bogie for single bogie W = 12500N, a = 5.65 mm and 1.77mm, the maximum pressure at the center point of the contact ellipse is given by:

$$P = \frac{3W}{2\pi ab} = \frac{12500 \times 3}{2\times\pi\times 0.00565\times 0.00177} = 596MPA \quad (34)$$

The principal stresses at the center of the surface of contact are calculated as:

5.1.3 Heat Flux Analysis at Contact Area

When wheel and rail are brought into contact under the action of the static wheel load, the area of contact and the pressure distribution are usually calculated with the Hertz's theory. When a wheel rolls on a rail, the contact area and the pressure distribution can be obtained by the Hertz theory. The normal pressure distribution is determined as follows:

$$P = Po\sqrt{1 - (\frac{x^2}{a^2} - \frac{y^2}{b^2})} \tag{35}$$

In the case of a infinitely long cylinder subjected to the normal load N/b'per unit length, the normal pressure distribution is:

$$P(x,y) = P_0 \times \sqrt{1 - \frac{x^2}{a^2}} \tag{36}$$

The maximum pressure P_0 is calculated from the normal contact force F by the following equation [25]:

$$P_O = \frac{3F}{2\pi a' b} \tag{37}$$

This model is often used for a simplified analysis of three-dimensional contact problems. The reference length a' for the transition from the three-dimensional to the two dimensional case:

$$a' = \frac{4}{3}.a \tag{38}$$

$$a' = \frac{4}{3}.a = \frac{4}{3}*5.65mm = 7.53mm$$

$$P_o = \frac{3F}{2\pi\, a' b} = \frac{3\times12500}{2\times\pi\times0.00177\times0.00753} = 448MPa$$

A particle in the rail surface is in contact with the wheel during a very short period. For calculation of the flash-temperature due to frictional heat, a very thin layer in the rail surface can be considered as the instantaneous affected zone.

The Péclet number can be related to the forward velocity *V0* (vehicle speed) and the thermal diffusivity κ. The effect of material properties is introduced by thermal diffusivity, which combines thermal conductivity λ, density ρ and specific heat capacity c:

$$p_e = \frac{a\mathrm{V}_o}{2k} \, , k = \frac{\lambda}{\rho c} \tag{39}$$

If Pe >10, the heat conduction occurs only perpendicular to the contact plane, i.e. in the vertical direction (z) [13]. This condition is basically valid for typical situations of the wheel rail system. Therefore, the longitudinal (x) and lateral (y) heat conduction can be neglected. The heat conduction equation in z-direction (rail depth) can be written by:

$$k \, \frac{\partial^2 T}{\partial z^2} = \frac{\partial T}{\partial t} \tag{40}$$

Which is a second-order partial deferential equation involving temperature rates of change with respect to the time and rail depth. The material particles in the contact patch are subjected to the frictional heat source q (t), while the wheel is passing the rail. Assuming zero temperature as the initial state, the boundary condition at time t can be written as:

$$\lambda \frac{\partial T}{\partial z} \, (Z = 0, t) = q(t) \tag{41}$$

The time parameter (t) can be substituted by the wheel position in longitudinal direction (x) using x = Vt. Therefore, the heat conduction equation (only in z direction) will include the wheel sweeping on rail in the longitudinal direction.

The dimensionless coordinates of each material particle in rail (2D) [14] can be represented by:

$$\xi = \frac{x}{a} \quad , \quad \zeta = \frac{z}{\delta} \tag{42}$$

Defining β as the thermal penetration coefficient and v_w as the wheel velocity by the sum of the forward velocity V_0 = 19.4m/s and sliding velocity Vs= 3 m/s, $\lambda = 50W/km$ and $\kappa = 1.518 \times \frac{10^{-5}m^2}{s}$ [14] then:

$$\beta = \sqrt{\lambda \rho c} = \frac{\lambda}{\sqrt{\kappa}} \tag{43}$$

$$= \frac{50W/km}{\sqrt{1.518\times10^{-5}m^2/s}}, \ \beta = 12{,}833.2$$

$$V_w = V_o + V_s \tag{44}$$

$$= 19.4 \text{ m/s} + 4\text{m/s}$$

$$V_w = \frac{23.4\ m}{s}$$

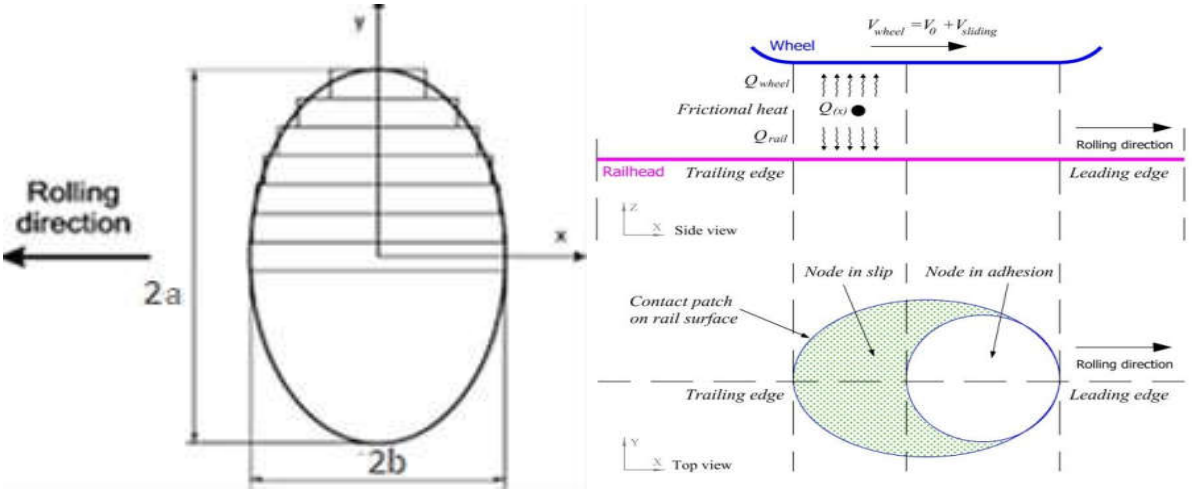

Figure 15 : Elliptical area of the contact and Calculation of the temperature in partial-slip rolling contact, the side and top views are shown.

The partition of heat that flows into wheel [14] is given by:

$$\varepsilon = \frac{\beta_w \sqrt{V_w}}{\beta_w \sqrt{V_w} + \beta_r \sqrt{V_o}} \tag{45}$$

Where subscripts w and r indicate the wheel and rail respectively. Tw and Tr are temperatures of the wheel and rail respectively and also ε is the heat partitioning coefficient.

$$\varepsilon_1 = \frac{\beta_w\sqrt{V_w}}{\beta_w\sqrt{V_w}+\beta_r\sqrt{V_o}} = \frac{12833.2\sqrt{23.4}}{12833.2\sqrt{23.4}+12833.2\sqrt{19.4}} = 0.5$$

Based on the Coulomb's friction law, the distribution of the tangential stress is given as follows:

$$\tau\,(x,y) = \mu P(x,y) \tag{46}$$

Where μ is the friction coefficient.

The heat flux distribution within the contact patch due to friction [8] is given as:

$$q(x,y) = \mu V_s P(x,y) \tag{47}$$

An analytical approximation is proposed in for the elliptical heat flow rate in the Hertzian contact:

$$q_{friction}(\xi) = fV_s\,P_o f(\xi) \tag{48}$$

The average heat flow rate at the surface of the rail is calculated in the following formula:

$$q(\xi) = \frac{\pi}{4}.\varepsilon_1\mu V_s P_o \tag{49}$$

$$\mathrm{q}(\xi) = \frac{\pi}{4}\varepsilon_1\mu V_s P_o = \frac{\pi}{4}[0.5 \times 0.58 \times 4 \times 448\mathrm{MPa}]$$

$\mathrm{q_{friction}}(\xi) = 408\mathrm{MW/m^2}$

And the average heat flow rate at the surface of the wheel will be calculated when $\mu = 0.58$

$$q(\xi) = (1-\varepsilon_1)\,\frac{\pi}{4}\mu V_s P_o \tag{50}$$

$$= (1-0.5)\frac{\pi}{4} \times 0.58 \times 3m/s \times 448MPa$$

$$q(\xi) = 408MW/m^2$$

Analysis of Heat flux and temperature at the contact area for vehicle speed of V_o= 19.4 m/s and slip velocity of 8 m/s.

Heat partitioning coefficient

$$\varepsilon_2 = \frac{\beta_w\sqrt{V_w}}{\beta_w\sqrt{V_w}+\beta_r\sqrt{V_o}} = \frac{12833.2\sqrt{27.4}}{12833.2\sqrt{26.4}+12833.2\sqrt{19.4}}$$

$$\varepsilon_2 = 0.51$$

The average heat flow rate at the surface of the rail is calculate when $\mu = 0.5$:

$$q_{friction}(\xi) = \frac{\pi}{4}.\varepsilon_2\mu V_s P_o$$

$$= \frac{\pi}{4}.\times 0.51 \times 0.5 \times 8m/s \times 448MPa$$

$q_{friction}(\xi)$= 720MW/m^2

As we calculated the average heat flow rate at the surface of the rail, then we calculate the average heat flow rate at the surface of the wheel will be:

$$q_{w\ friction}(\xi) = (1-\varepsilon_2)\frac{\pi}{4}\mu V_s P_o$$

$$= (1-0.512)\frac{\pi}{4}0.5 * \frac{7m}{s} * 448MPa$$

$$\dot{q}_{friction}(\xi) = 686MW/m^2$$

Analysis of Heat flux and temperature at the contact area for vehicle speed of V_o= 19.4 m/s and slip velocity of 12 m/s.

Heat partitioning coefficient of wheel and rail during rolling sliding contact is:

$$\varepsilon_3 = \frac{\beta_w\sqrt{V_w}}{\beta_w\sqrt{V_w}+\beta_r\sqrt{V_o}} = \frac{12833.2\sqrt{\frac{31.4m}{s}}}{12833.2\sqrt{\frac{31.4m}{s}}+12833.2\sqrt{19.4}}$$

$$\varepsilon_3 = 0.52$$

The average heat flow rate at the surface of the rail is calculated when $\mu = 0.4$:

$$q_{friction}(\xi) = \frac{\pi}{4}.\varepsilon_3 \mu V_s P_o$$

$$= \frac{\pi}{4}.0.52 \times 0.4 \times 12\text{m/s} \times 448\text{MPa}$$

$$q_{friction}(\xi) = 877\text{MW/m}^2$$

As we calculated the average heat flow rate at the surface of the rail, then we calculate the average heat flow rate at the surface of the wheel will be:

$$q(\xi) = (1 - \varepsilon_3)\frac{\pi}{4}\mu V_s P_o$$

$$= (1 - 0.52)\frac{\pi}{4} * 0.4 * \frac{12\text{ m}}{\text{s}} * 448\text{MPa}$$

$$q_{w\,friction}(\xi) = 811\text{ MW/}m^2$$

Analysis of Heat flux and temperature at the contact area for vehicle speed of V_o= 19.4 m/s and slip velocity of 16m/s

Heat partitioning coefficient of wheel and rail during rolling sliding contact is:

$$\varepsilon_4 = \frac{\beta_w\sqrt{V_w}}{\beta_w\sqrt{V_w}+\beta_r\sqrt{V_o}} = \frac{12833.2\sqrt{\frac{35.4\text{m}}{\text{s}}}}{12833.2\sqrt{\frac{35.4\text{m}}{\text{s}}}+12833.2\sqrt{19.4}}$$

$$\varepsilon_4 = 0.53$$

The average heat flow rate at the surface of the rail is calculated when $\mu = 0.3$:

$$q_{friction}(\xi) = \frac{\pi}{4}.\varepsilon_4 \mu V_s P_o$$

$$= \frac{\pi}{4}.0.53 \times 0.3 \times 15\text{m/s} \times 448\text{MPa}$$

$$q_{friction}(\xi) = 894\text{MW/m}^2$$

As we calculated the average heat flow rate at the surface of the rail, then we calculate the average heat flow rate at the surface of the wheel will be:

$$q_{w\,friction}(\xi) = (1-\varepsilon_4)\frac{\pi}{4}\mu V_s P_o$$

$$= (1-0.53) * \frac{\pi}{4} * 0.3 * \frac{16m}{s} * 448MPa$$

$$q_{w\,friction}(\xi) = 841WM/m^2$$

5.1.4 Temperature Rise Calculation in the 3D Wheel-Rail Contact Problem

Using finite element method, a numerical model is developed in this paper for the temperature calculation in a more realistic way. During the rolling/sliding contact between the wheel and rail, heat is generated at the contact surface due to friction. A 3D transient FE model is built to examine the coupled mechanical-thermal behavior of the contact bodies with arbitrary geometries under frictional rolling contact. The analytical methods, for calculation of the flash-temperature due to frictional heat, a very thin layer in the rail surface can be considered as the instantaneous affected zone. However, the temperature solution is will be sight for the 3D contact problem with partial slip using a transient time integration. The heat flux is generated in the slip region only. Rolling contact with frictional heat generation is simulated with the wheel running with a constant speed on the rail. A particle in the rail surface is in contact with the wheel during a very short period. The maximum temperature occurs at the trailing edge of the contact patch that was already been given by Blok [19]. Assuming that the only source of heat over the area is friction, friction-induced temperature it can be used as a simple estimate for the friction-induced temperature of wheel and rail.

$$T_{max} = \frac{1.253.\varepsilon.\mu.V_s.P_O}{\beta_r}\sqrt{\frac{a}{V_r}} \tag{51}$$

Analysis of induced temperature at the contact area for vehicle speed of $V_o = V_r = 19.4$m/s, slide velocity of (V_s) = 4m/s, thermal partition of wheel β_w = 12833.2 and temperature rise for μ = 0.58

$$T_{max} = \frac{1.253.\varepsilon_1.\mu.V_s.P_O}{\beta_r}\sqrt{\frac{a}{V_r}} = \frac{1.253\times0.5\times0.58\times4\ m/s\times448MPa}{12833.2}\sqrt{\frac{0.00565}{19.4}}$$

$= 866℃$

And the friction-induced temperature of wheel is

$$T_{max} = \frac{1.253.\varepsilon_1.\mu.V_s.P_O}{\beta_w}\sqrt{\frac{a}{V_w}} \tag{52}$$

$$= \frac{1.253 \times 0.5 \times 0.58 \times 4\ \text{m/s} \times 448\text{MPa}}{12833.2}\sqrt{\frac{0.00565}{23.4}} = 788℃$$

With similar procedure the surface temperature over the contact area are calculated for 8 12m/s and 16 slip velocities for vehicle running 19.4 m/s. The analysis is carried as follow; Friction-induced temperatures of rail at 8m/s slip velocity and temperature rise for $\mu = 0.5$ is

$$T_{max} = \frac{1.253.\varepsilon_2.\mu.V_s.P_O}{\beta_r}\sqrt{\frac{a}{V_r}} = \frac{1.253\times0.512\times0.5\times8\ \text{m/s}\times448\text{MPa}}{12833.2}\sqrt{\frac{0.00565}{19.4}}$$

$=1522℃$

The friction-induced temperature of wheel at the same slip velocity and the same temperature rise

$$T_{max} = \frac{1.253.\varepsilon_2.\mu.V_s.P_O}{\beta_w}\sqrt{\frac{a}{V_w}} = \frac{1.253\times0.49\times0.5\times8\text{m/s}\times448\text{MPa}}{12833.2}\sqrt{\frac{0.00565}{27.4}}$$

$=1231℃$

Friction-induced temperatures of rail at 12m/s slip velocity and temperature rise for $\mu = 0.4$ is

$$T_{max} = \frac{1.253.\varepsilon_3.\mu.V_s.P_O}{\beta_r}\sqrt{\frac{a}{V_r}} = \frac{1.253\times0.52\times0.4\times12\frac{\text{m}}{\text{s}}\times448\text{MPa}}{12833.2}\sqrt{\frac{0.00565}{19.4}}$$

$= 1863℃$

The friction-induced temperature of wheel at the same slip velocity and the same temperature rise.

$$T_{max} = \frac{1.253.\varepsilon_3.\mu.V_s.P_O}{\beta_w}\sqrt{\frac{a}{V_w}} = \frac{1.253\times0.48\times0.4\times12\frac{m}{s}\times448MPa}{12833.2}\sqrt{\frac{0.00565}{31.4}}$$

$$= 1246℃$$

Friction-induced temperatures of rail at 16m/s slip velocity and temperature rise for $\mu = 0.3$

$$T_{max} = \frac{1.253.\varepsilon_3.\mu.V_s.P_O}{\beta_r}\sqrt{\frac{a}{V_r}} = \frac{1.253\times0.53\times0.3\times16\frac{m}{s}\times448MPa}{12833.2}\sqrt{\frac{0.00565}{19.4}}$$

$$= 1898℃$$

The friction-induced temperature of wheel at the same slip velocity and the same temperature rise.

$$T_{max} = \frac{1.253.\varepsilon_3.\mu.V_s.P_O}{\beta_w}\sqrt{\frac{a}{V_w}} = \frac{1.253\times0.47\times0.3\times16\frac{m}{s}\times448MPa}{12833.2}\sqrt{\frac{0.00565}{35.4}}$$

$$= 1352℃$$

5.1.5 Rail flash-temperature

Results of temperature rise generated by frictional heat were deduced from the numerical simulation. A summary of the maximum flash-temperature for various traction coefficients are given in Table 1. Assuming zero temperature in the materials at the beginning of the simulations, the results are representative of the temperature rise generated by friction.

Table 1: Rail flash-temperature

Traction	0.58	0.5	0.4	0.3
Sliding velocity	4	8	12	16
Flash temperature	827	1376.5	1554	1625

5.1.6 Heat convection

Outside the area of contact, heat flows from the wheel into ambient air by convection at the free surfaces. With the heat transfer coefficient with varying sliding velocity [27]

$$\mathrm{h} = \frac{N_u \times k_{air}}{r_w} \tag{53}$$

$$N_u = 0.037 \times {R_e}^{0.8} \tag{54}$$

$$R_e = \frac{V_{air} \times r_w}{v_{air}} \tag{55}$$

$$V_{air} = K_v \times V_o \tag{56}$$

Depending on the property of air for vehicle speed of V_o= 19.4 m/s at 1atm and slip velocity of 4.00 m/s

K_v =0.12, k_{air} = 0.025, $v_{air} = 34.5 \times 10^{-6}\ m^s/s$

$V_{air} = K_v \times V_o$ = 0.12 *19.4m/s = 2.328 m/s

$R_e = \frac{V_{air} \times r_w}{v_{air}} = \frac{2.328 * 0.42}{34.5 \times 10^{-6}}$ = 28340.9

$N_u = 0.037 \times {R_e}^{0.8} = 0.037 \times 28340.9^{0.8}$ = 134.9

N_u = 134.9

$$h = \frac{N_u \times k_{air}}{r_w} = \frac{134.9 \times 0.025}{0.33} = 8.3 \frac{W}{m^2 K}$$

Table 2: Heat convection along wheel contact

Sliding velocity	19.4	23.4	27.4	31.4	35.4
Heat convection	$10.3 \frac{W}{m^2 K}$	$12 \frac{W}{m^2 K}$	$13.5 \frac{W}{m^2 K}$	$15 \frac{W}{m^2 K}$	$16.5 \frac{W}{m^2 K}$

5.1.7 Normal and Tangential Stress Distribution in Wheel –Rail Contact

The effects of vehicle speed, all types of creep ages and elliptical contact area are taken into consideration [9]. When the level of creepage is not too high (approximately less than 1%), the Carter's equation considers almost a linear relationship between the creepage and the creep force. For high creepages and for the full-slip contact a nonlinear relationship exists between the mentioned parameters, while the maximum creep force is limited to *fN*. Various tangential loads (*F*) are simulated by applying different values of the traction coefficient on wheel (μ):

$$\mu = \frac{F}{N} \leq f = 0.6 \tag{57}$$

where, *f* denotes the friction coefficient. Four values of the traction coefficient i.e. 0.3, 0.4 and 0.58 are considered to model different levels of partial slip. The greatest coefficient (μ*=0.58*) simulates an almost full-slip contact from equation (57)

Tangential load when $\mu = 0.58$

$$\mu = \frac{F}{N} \leq f = 0.6 F = N\mu = 12500 \times 0.58 = 7250 kN$$

Table 3: Normal and Tangential Stress Distribution in Wheel –Rail Contact

Traction coefficient	0.58	0.5	0.4	0.3
Tangential load	7250N	6250N	5000N	3750

5.1.8 Finite Element (FE) Couple of Thermo-Mechanical Analysis

To perform the objective and scope of the thesis, a 3D elastic finite element model is used. All the finite element models are built using ANSYS software. The general procedure is first, the 3D geometry model is transferred or imported to ANSYS software and then meshed with ANSYS workbench. The meshing at the contact location is refined very well for efficient and accurate computation. The contact between rail and wheel is modeled using ANSYS workbench. Therefore, lateral loads to the system are considered and the rotational effect of the wheels is also considered. The coefficient of friction at the wheel-rail rolling contact varies according to the track and environmental conditions. Based on these conditions the rolling contact traction coefficient, μ= 0.3, 0.4, 0.5 and 0.58 are used in the FE analysis for this investigation. The rail and wheel material properties are assumed to be the same but different carbon content, and a bilinear kinematic hardening elastic material model is used in ANSYS workbench. Boundary and loading conditions are applied to the model. The rail is fixed at both ends and bottom of the rail to prevent rigid body motion of the whole system.

Table 4: Mechanical material properties of wheel and rail steel

Material properties	**Value**
Poisons ratio	0.3
Young's modulus	197.5 GPA
Tangent modulus	15000MPa
Yield strength	550 MPa
Tensile Ultimate strength	880 MPa
Tensile yield strength	540 MPa
Isotropic thermal conductivity	46.5
Material density	7785Kg/m

Table 5 : Material parameters for quenched and tempered wheel steel R7 at different temperatures used in calculate

T (°C)	ρ (kg m^{-3})	E (GPa)	ν	σ_Y (MPa)	E_K (GPa)	α (10^{-6} °C^{-1})	c (J kg^{-1} °C^{-1})	λ (W m^{-1} °C^{-1})
0	7850	210.0	0.2830	570.0	15.00	11.60	450.0	47.10
100	7818	203.8	0.2860	560.0	15.00	12.20	487.5	47.10
200	7785	197.5	0.2900	550.0	15.00	12.80	525.0	45.30
300	7753	191.3	0.2940	540.0	13.50	13.40	575.0	43.00
400	7720	185.0	0.2980	530.0	12.00	14.00	625.0	40.00

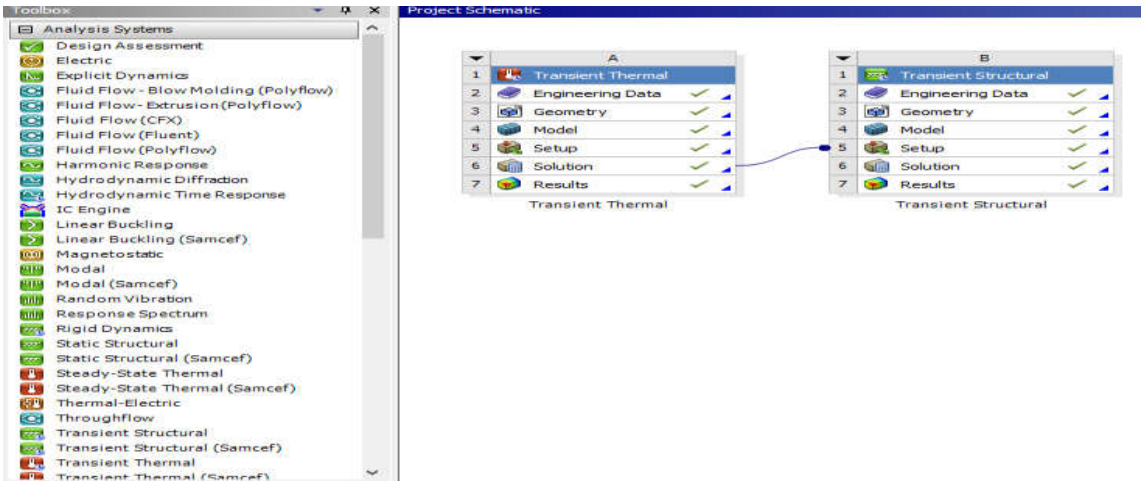

Figure 16 : stepwise solving ANSYS workbench for couple of thermos-mechanical analysis

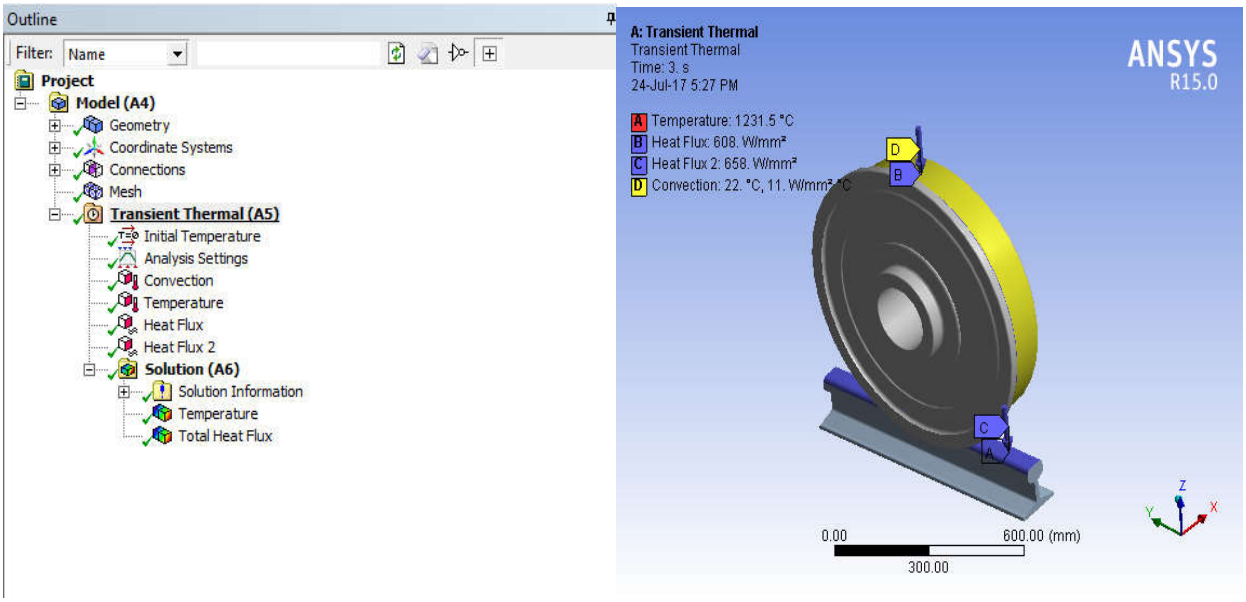

Figure 17: Loading and boundary condition at transient thermal tree chart

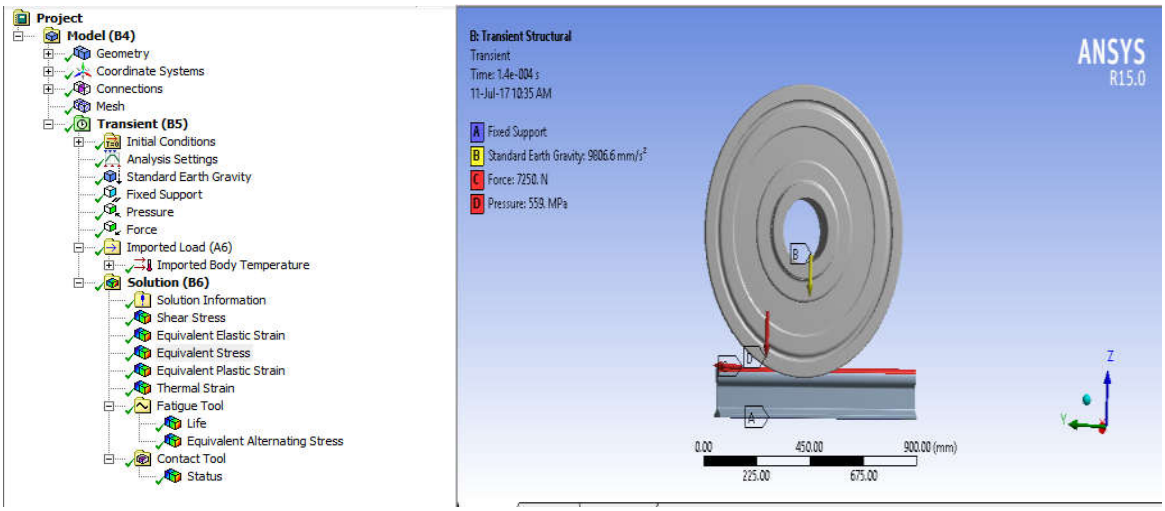

Figure 18: Mechanical load setting over imported contact surface thermal load for combined

5.1.9 Meshing

In the finite element analysis the basic concept is to analyze the structure, which is an assemblage of discrete pieces called elements, which are connected, together at a finite number of points called nodes. A network of these elements is known as a mesh. Meshing is discretizing the solid object to finest parts to perform the analysis to get the precise value at each and every elements of the meshed object. Since wheel and rail a 3D element the appropriate meshing method will be volume mesh so that all the volume of the wheel –rail is discretized to the smallest part of the wheel –rail. After this the object is ready to be analyzed by setting the analysis on the ANSYS work bench.

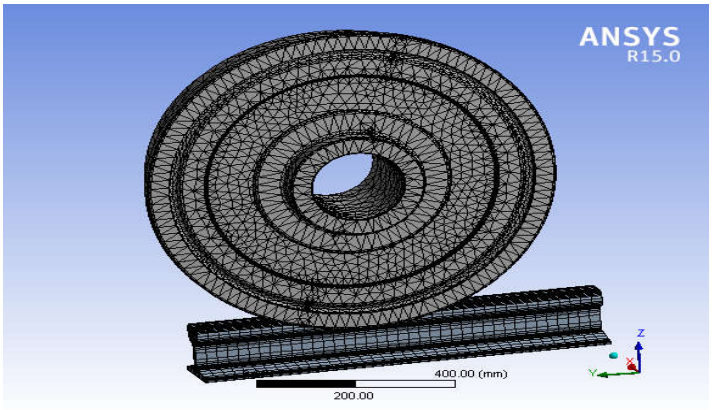

Figure 19 : Finite element Mesh of wheel –rail contact rail-wheel assembly

CHAPTER SIX

6.1 RESULTS AND DISCUSION

6.1.1 Mechanical load stress and strain analysis

The main causes of mechanical loads are tangential and normal force. Based on analytical result the tangential force considering only longitudinal direction is 2.5KN and axle load of 25KN the distributed equally left and right wheel. Duration of applied load for simulation is the time requires crossing a contact area. The contact area is considered symmetrical.

Stress, strain and stress life over contact area is presented in figures bellow.

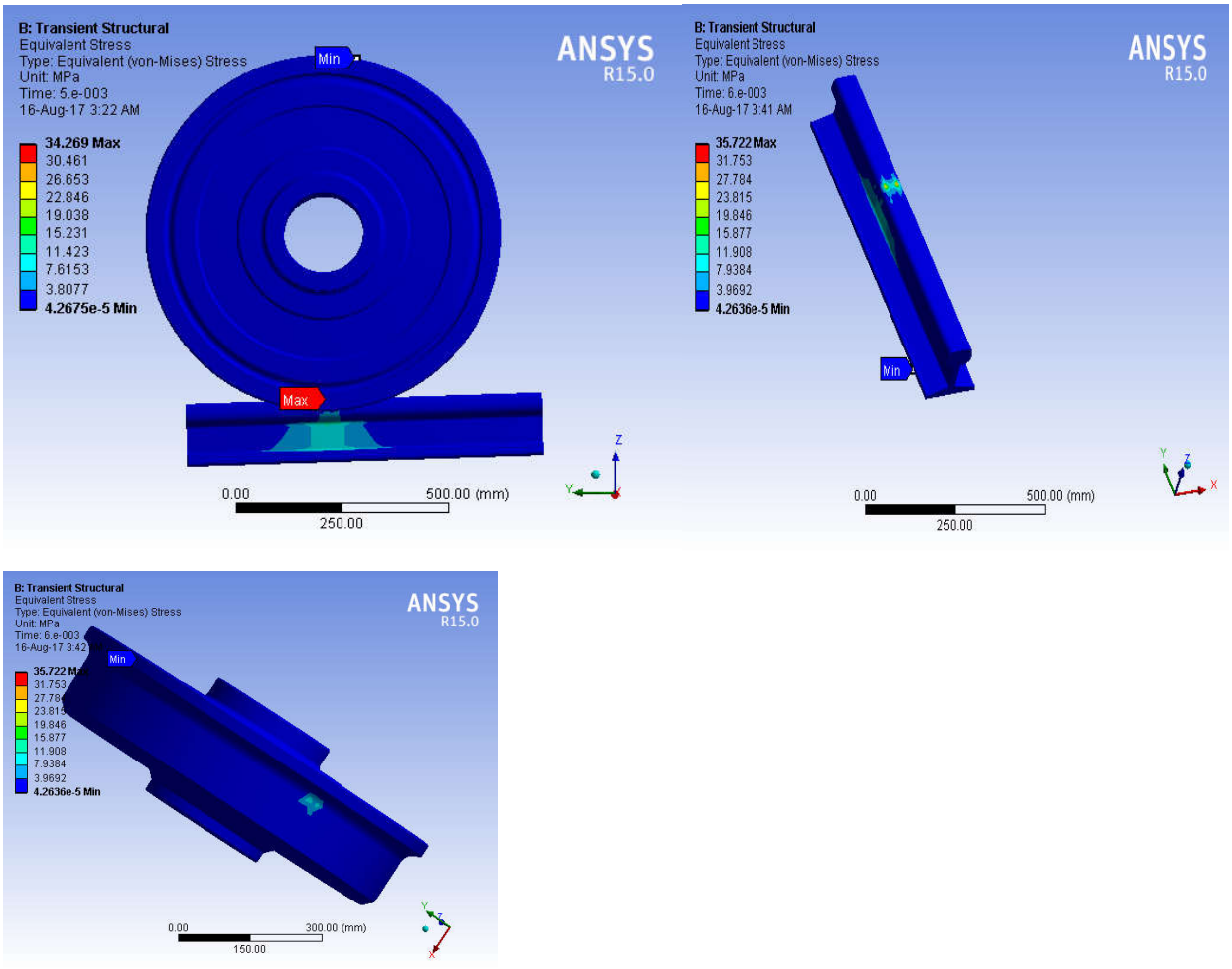

Figure 20 **:** Contact area stress life during mechanical load only

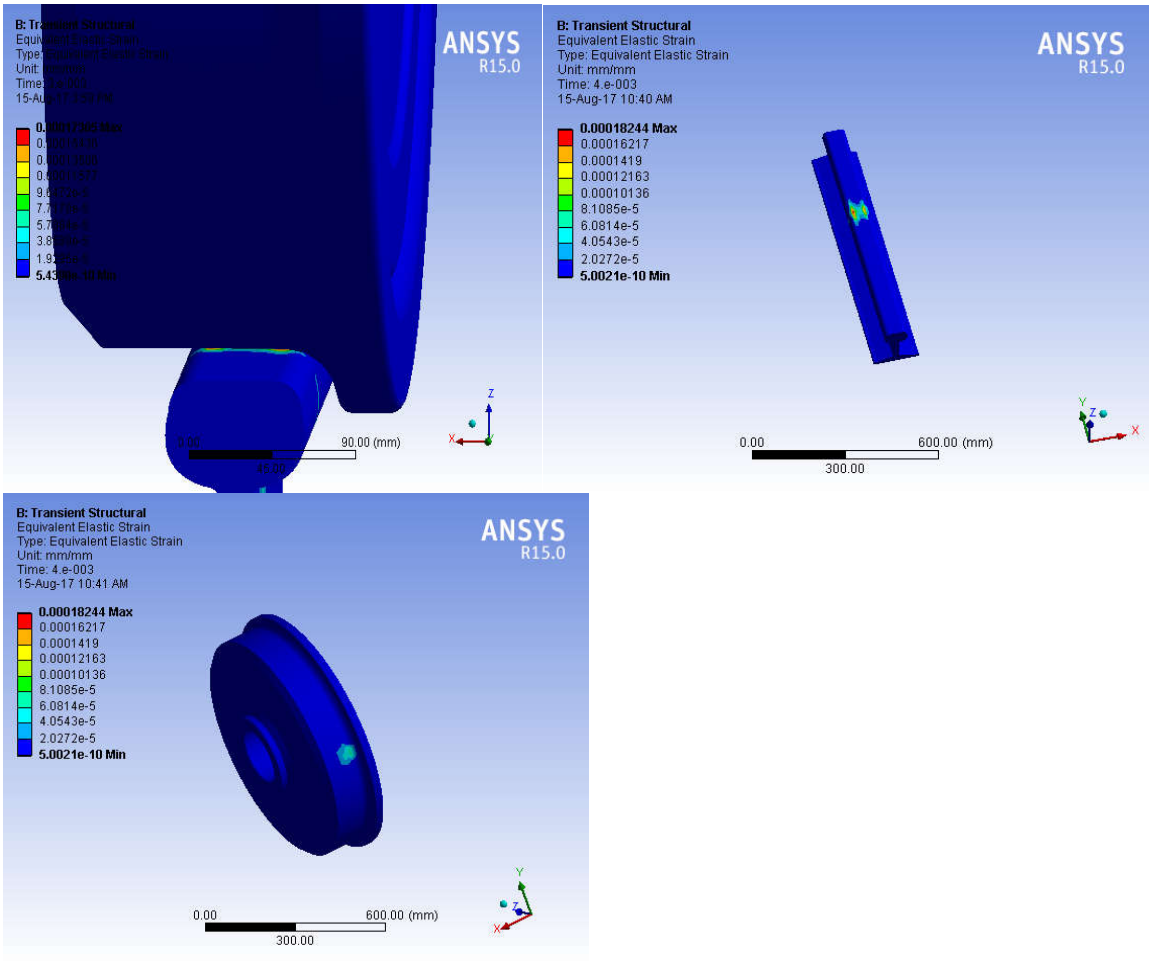

Figure 21 : Elastic strain at contact area due to mechanical load

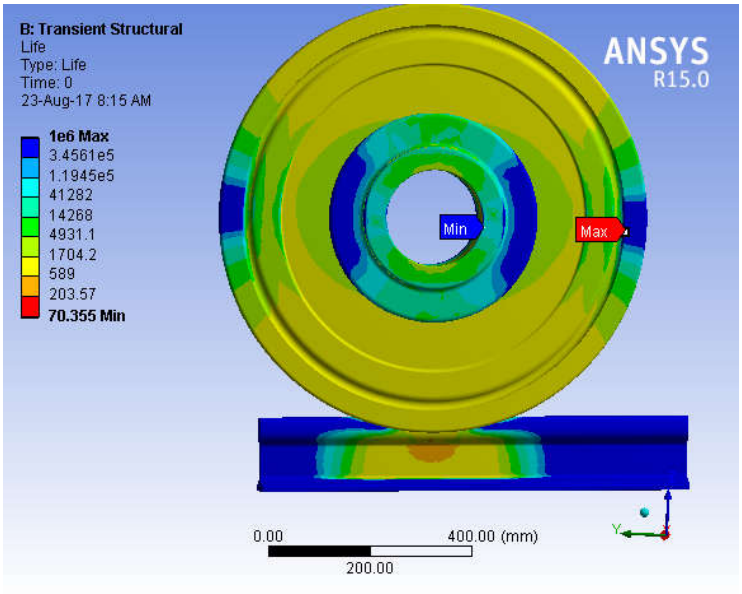

Figure 22 : Contact area stress life during mechanical load only

6.1.2 Thermal stress analysis

The source of heat generation at the contact area between rail and wheel is friction force. The sliding between wheel and rail causes frictional heating of both bodies. The maximum surface temperature during rolling contact of railway wheels with sliding friction is estimated using Blok's flash temperature formula. In addition for determining temperature rise of these components, the heat partition factor of rail and wheel is added on analysis. The results can be summarized in the following Tables.

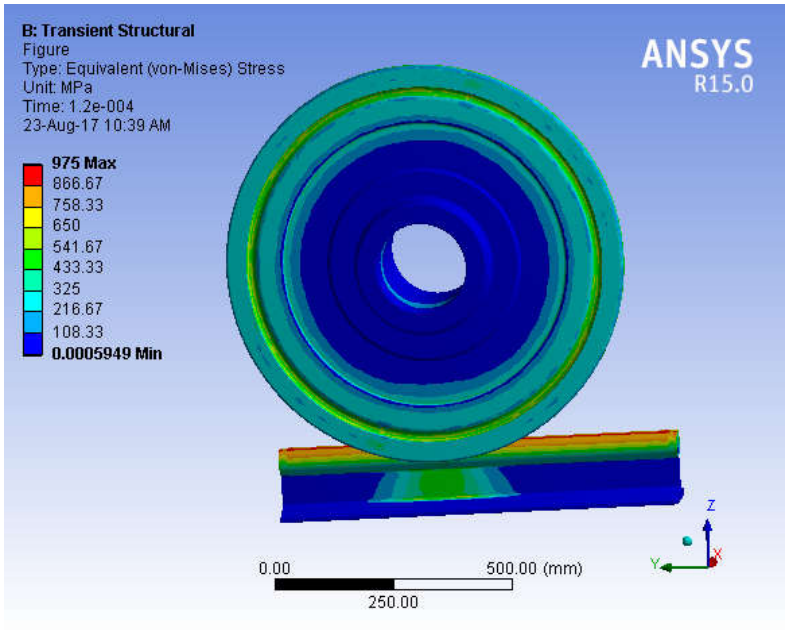

Figure 23 : Contact area thermal stress for 4 m/s slip velocity simulation

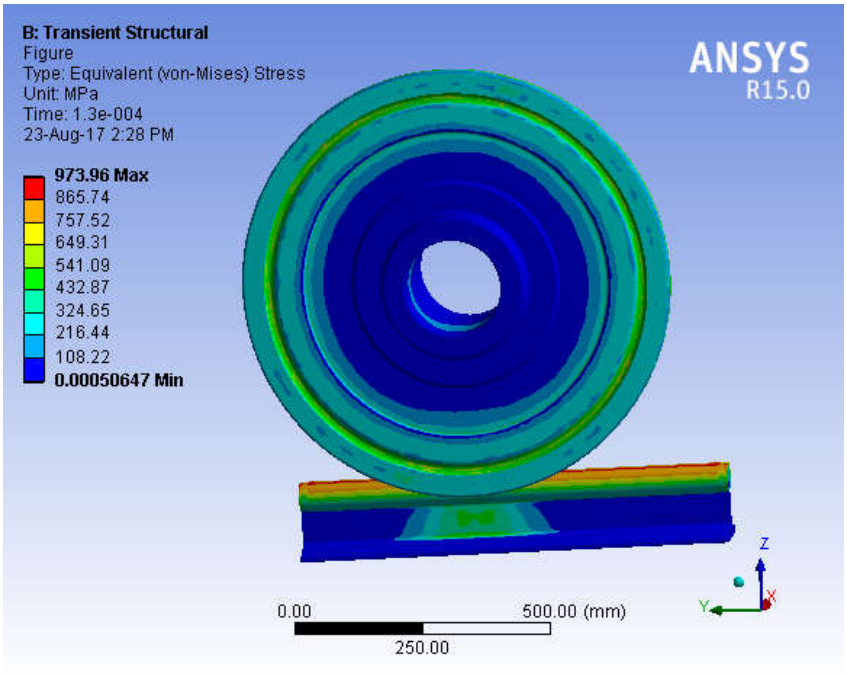

Figure 24 **:** Contact area thermal stress for 4 m/s slip velocity simulation

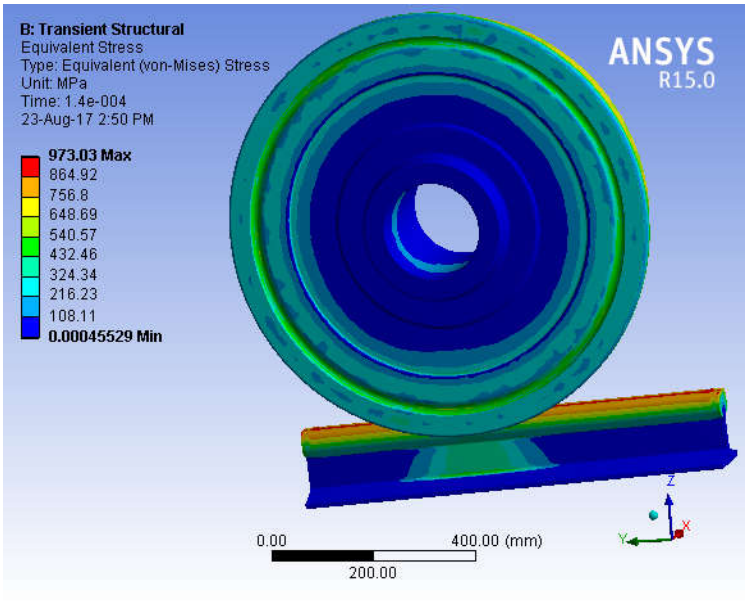

Figure 25 : Contact area thermal stress for 12 m/s slip velocity simulation

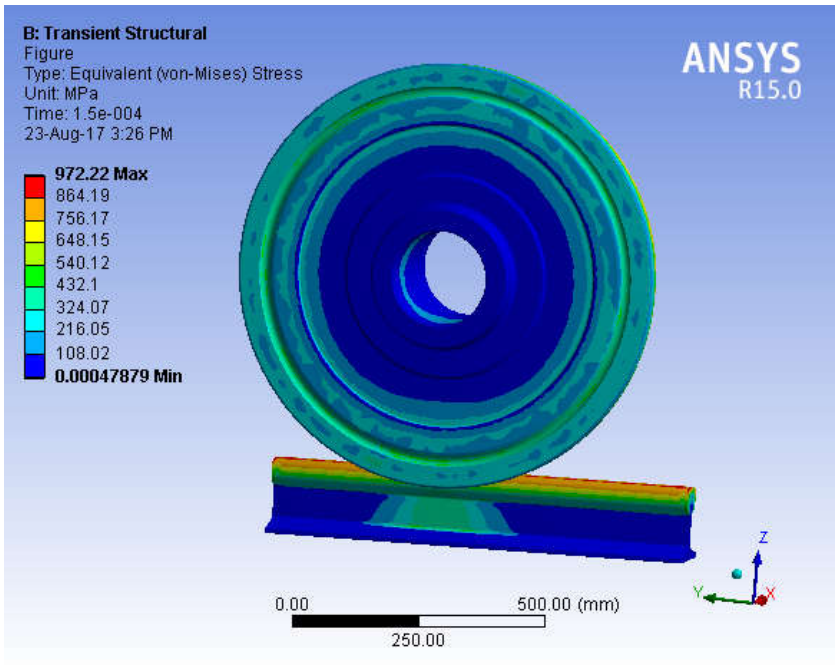

Figure 26 : Contact area thermal stress for 16 m/s slip velocity simulation

6.1.3 Thermo-Mechanical Couple Analysis

By selecting a time-step during the simulation, 3D distributions of the pressure and heat flux are applied. The longitudinal and lateral axes on the rail surface are normalized relative to the semi-axes *a,* and *b*, respectively. It should be noted that the wheel is located at $x=0$, while the leading edge and trailing edge of the contact patch are at $x=a$, and $x=-a$, respectively.

The longitudinal distributions of the pressure and tangential stress on the rail surface are demonstrated for various tractive efforts. As can be seen in the calculation, the level of traction coefficient did not influence the pressure distributions significantly. The effect of the sliding on the temperature rise, thermal strain, residual stress and residual strain under wheel-rail sliding-rolling contact are studied.

Table 6: Summary of loading condition for coupled thermal and mechanical simulation

Traction coefficient	Applied load at contact area			
	Mechanical load		Thermal load	
	Normal load pressure	Tangential load	Maximum flash surface temperature	
	596MPa			Slip velocity
0.58	>>	7250	827	4
0.5	>>	6250	1376	8
0.4	>>	5000	1554	12
0.3	>>	6250	1625	16

According to the input data the results showed are from mechanical - thermal load coupling analysis over contact area for single pass. Symmetric contact behavior is model and all loads are applied to the contact region. Depending on the above inputs surface temperatures it can be analyzed, equivalent von misses strain, equivalent von misses stress, and thermal strain, shear stress, and alternating equivalent stress are conducted at below

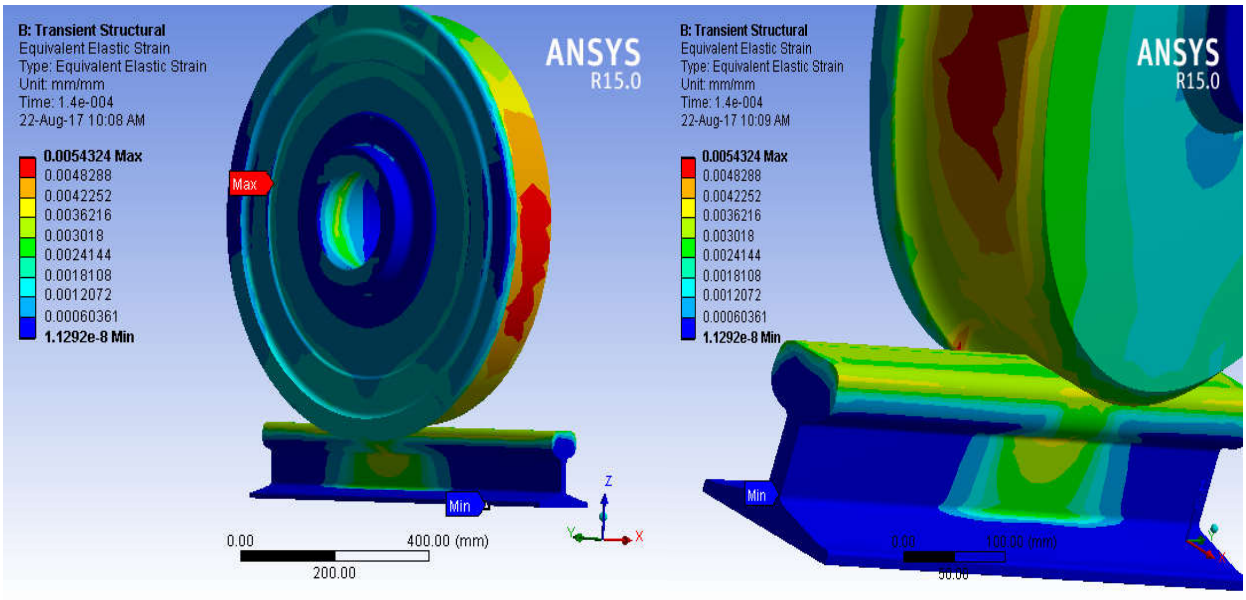

Figure 27 **:** Equivalent von Mises strain at 4m/s sliding velocity and traction coefficient of μ=0.58 simulation

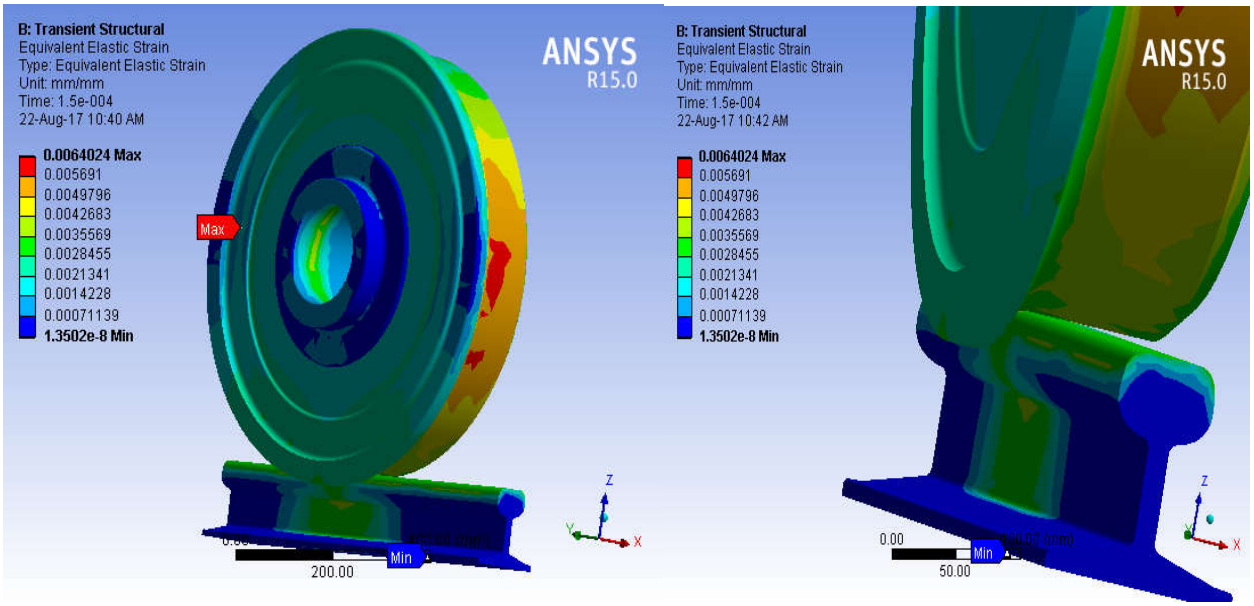

Figure 28 : Equivalent von Mises strain at 8 m/s sliding velocity and traction coefficient of μ=0.5 simulation

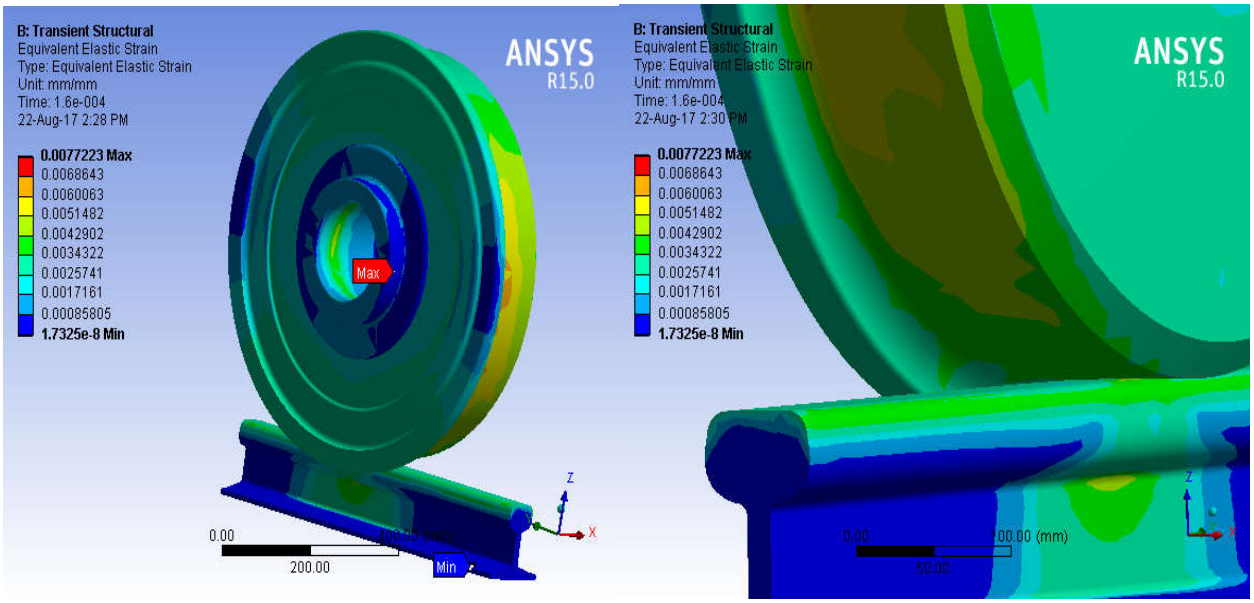

Figure 29 : Equivalent von Mises strain at 12m/s sliding velocity and traction coefficient of μ=0.4 simulation

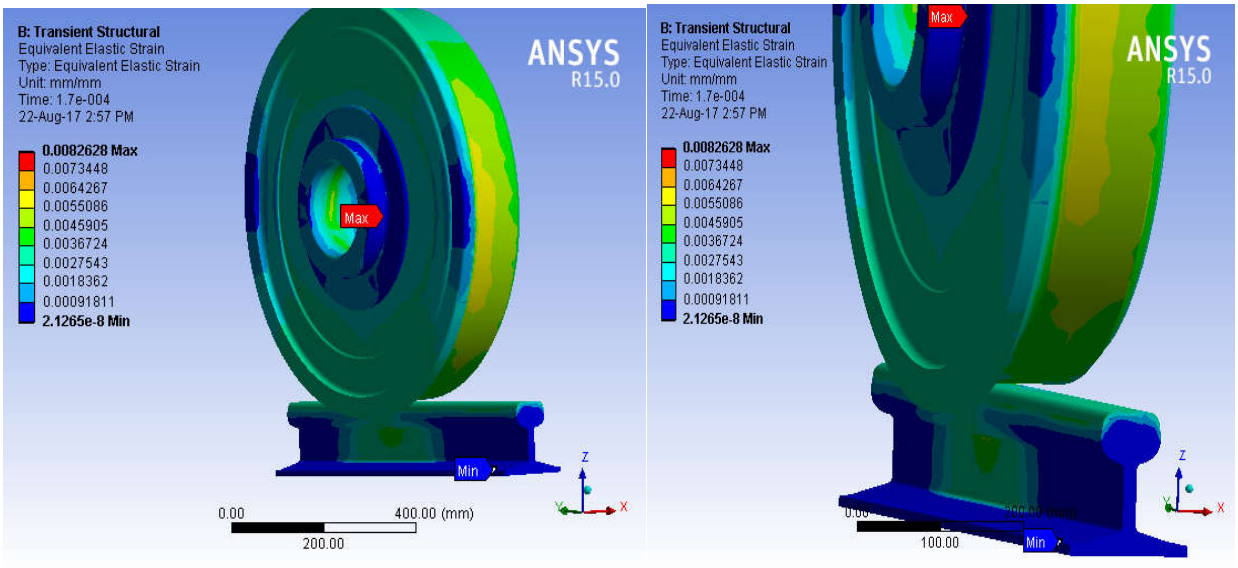

Figure 30 : Equivalent von Mises strain at 16m/s sliding velocity and traction coefficient of μ=0.3 simulation

The investigation results show that the thermally affected zone exists mainly in a very thin layer of material under the rail contact surface during the rolling-sliding contact. 0.0054324 is the maximum strain with the sliding velocity of 4 and traction coefficient of 0.58. The residual stresses induced by the frictional heat in the surface layer of rail appear to be tensile. When the maximum heat flux is applied, the frictional heat has a significant influence on the residual stresses and residual strains of rail and wheel. The present paper develops a thermo-mechanical coupling model of wheel-rail rolling-sliding contact, and the showed results can help to understand the mechanism of wheel/rail frictional thermal fatigue. Elastic strain resulted due to contact stress lower than elastic limit of the material.

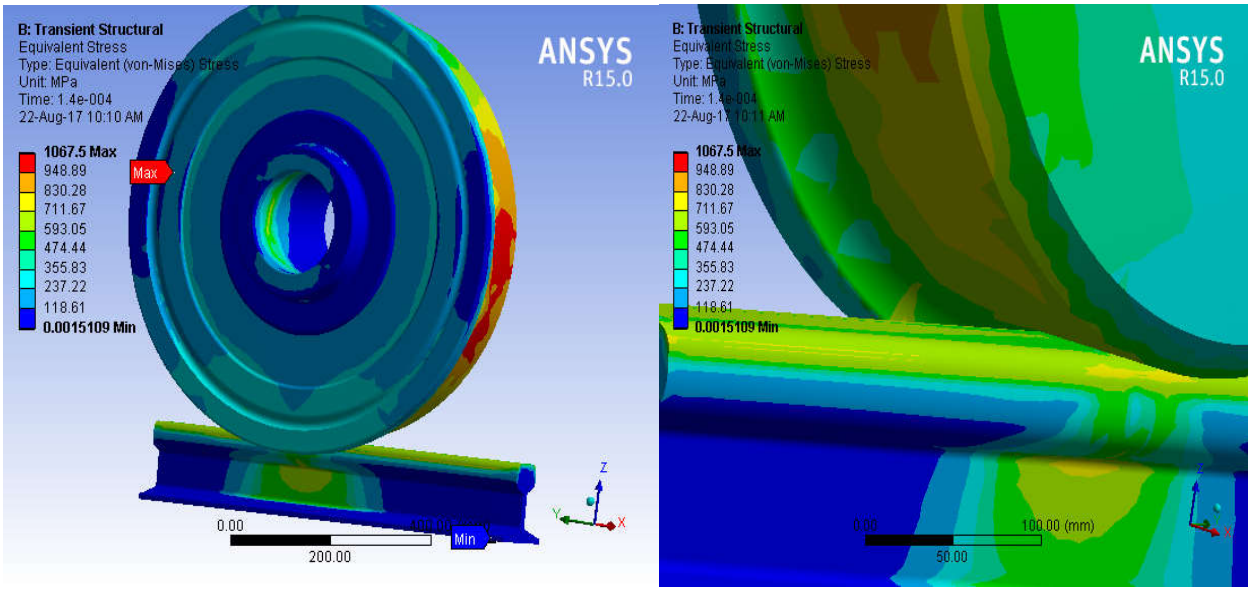

Figure 31 : Equivalent von Mises stress at 4m/s sliding velocity and traction coefficient of μ=0.58 simulation

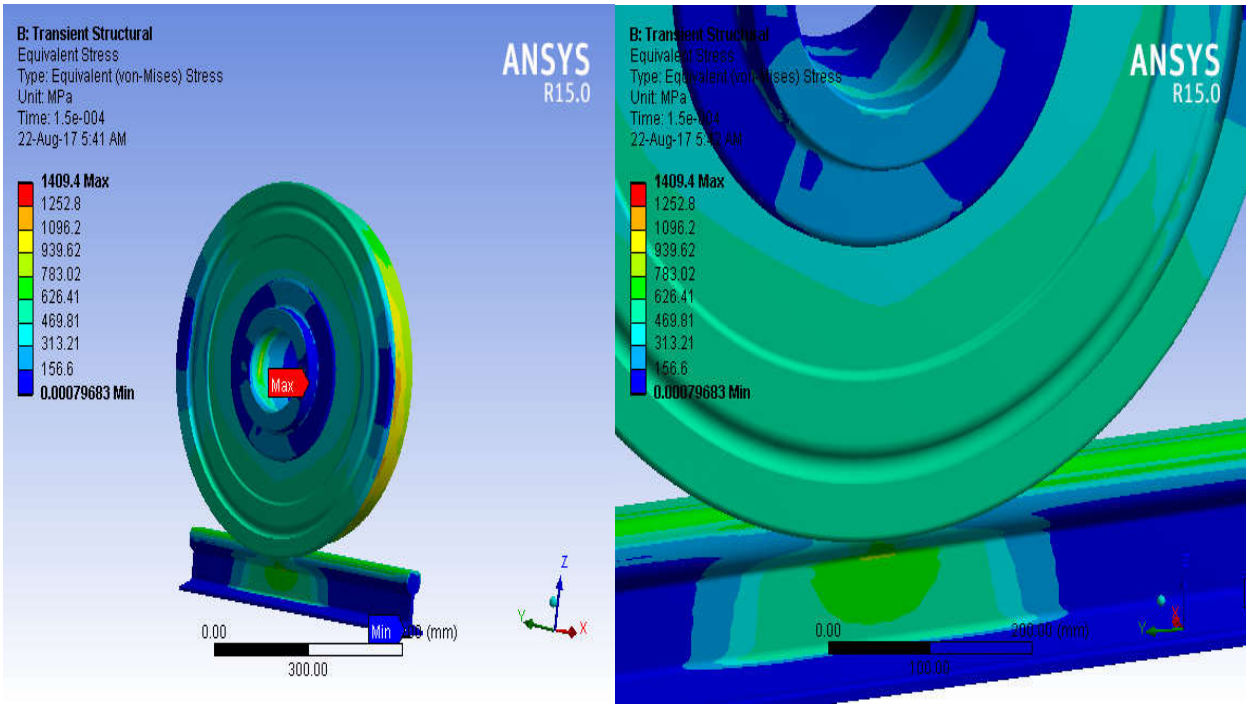

Figure 32 : Equivalent von Mises stress at 8 m/s sliding velocity and traction coefficient of μ=0.5 simulation

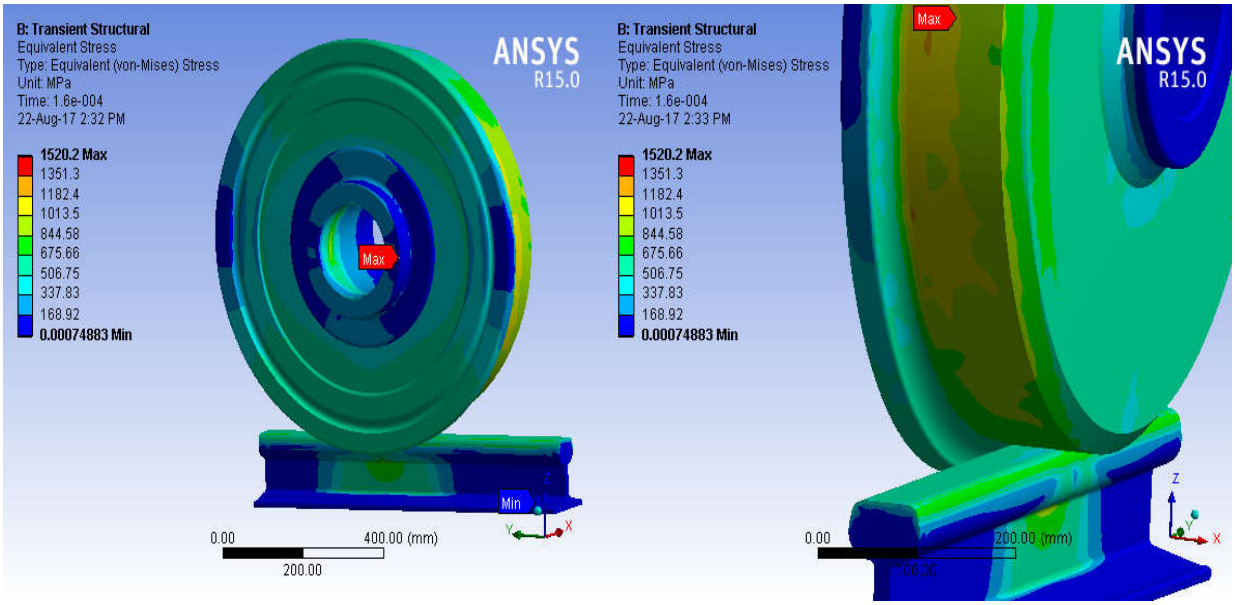

Figure 33 : Equivalent von Mises stress at 12 m/s sliding velocity traction coefficient of μ=0.4 simulation.

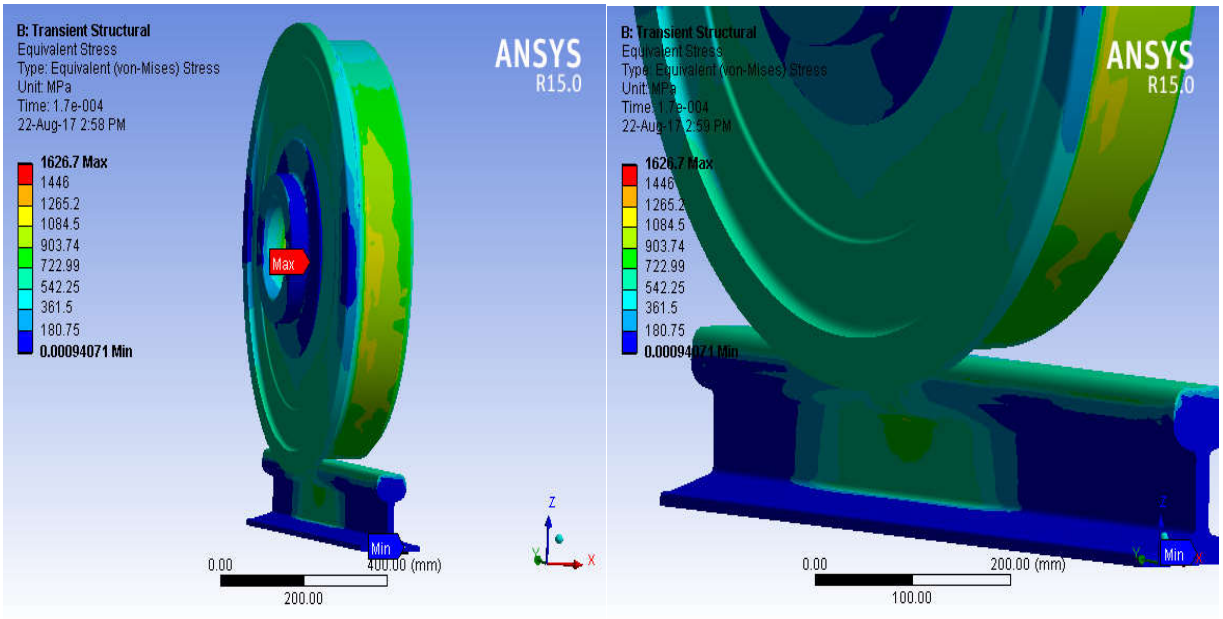

Figure 34 : Equivalent von Mises stress at 16m/s sliding velocity traction coefficient of μ=0.3 simulation

The equivalent von misese stresses in the four case of analysis is greater than the yield strength of material in combined load analysis. Even if critical stress points confined in few area, the existence of thermal load because of slippage affects the strength of the materials.

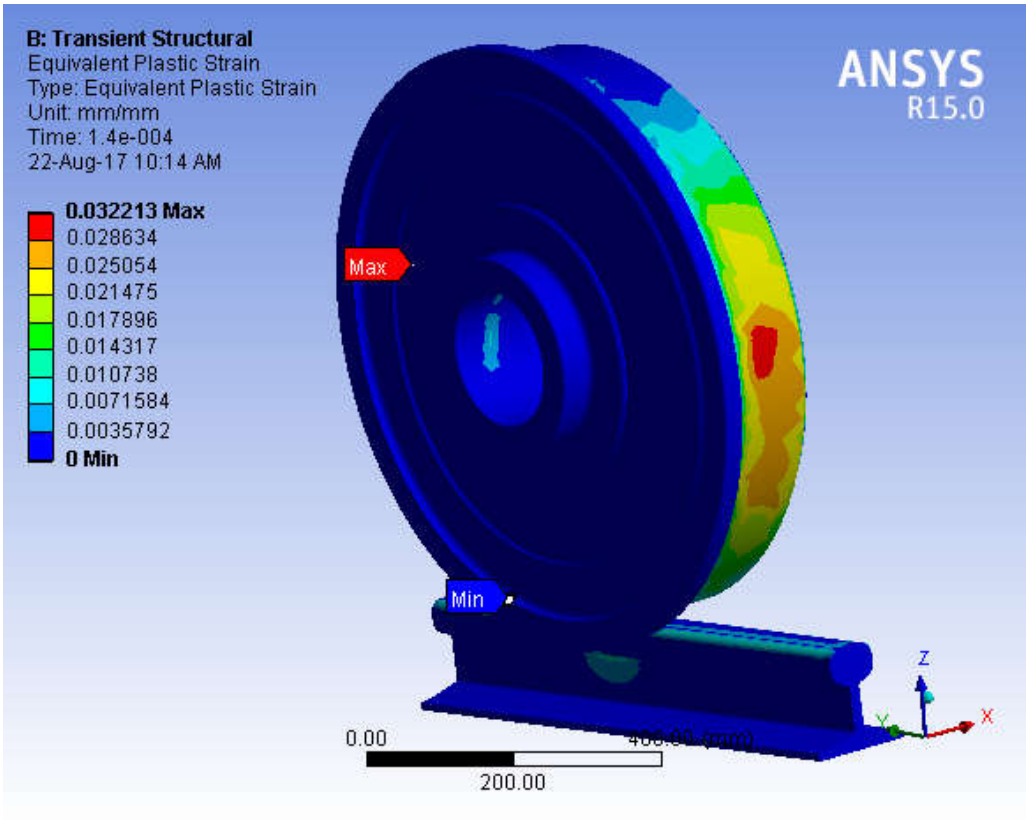

Figure 35 : Equivalent plastic strain at 4 m/s sliding velocity traction coefficient of μ=0.58 simulation

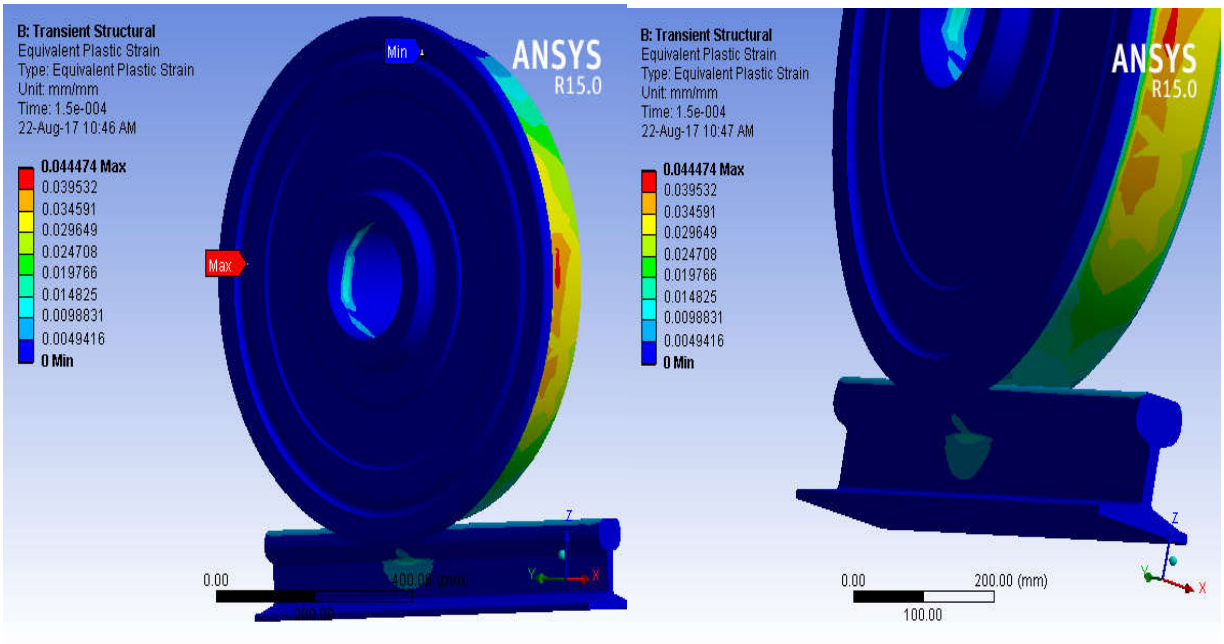

Figure 36 : Equivalent plastic strain at 8 m/s sliding velocity traction coefficient of μ=0.5 simulation

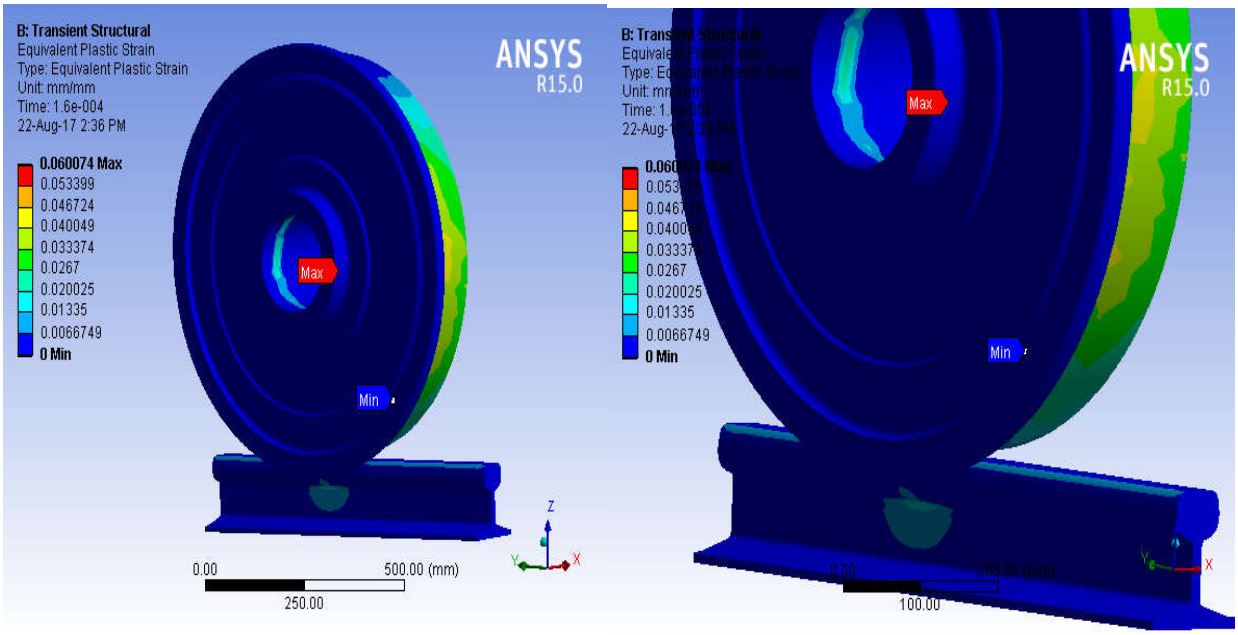

Figure 37 : Equivalent plastic strain at 12 m/s sliding velocity traction coefficient of μ=0.4 simulation

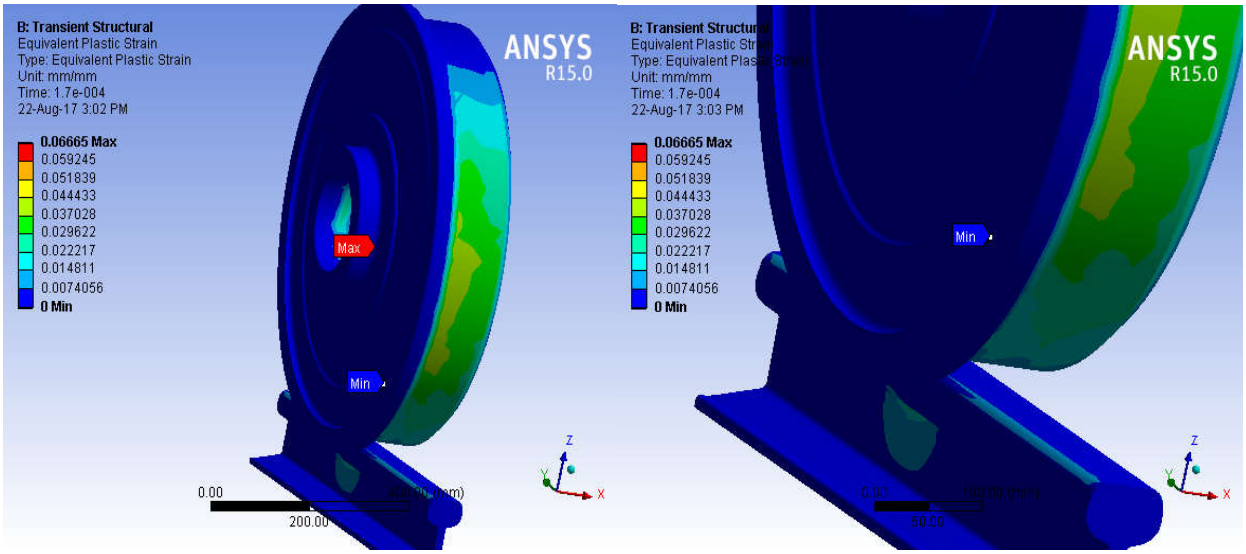

Figure 38 : Equivalent plastic strain at 16m/s sliding velocity traction coefficient of μ=0.3 simulation

Thermal strain created in the contact by presence of contact frictional heating. The thermal strain at contact will be greater and the stress life on contact area material is be short. Although the analysis type is the same (coupled analysis), because material properties are temperature dependent with their thermal deformations, the different results were achieved.

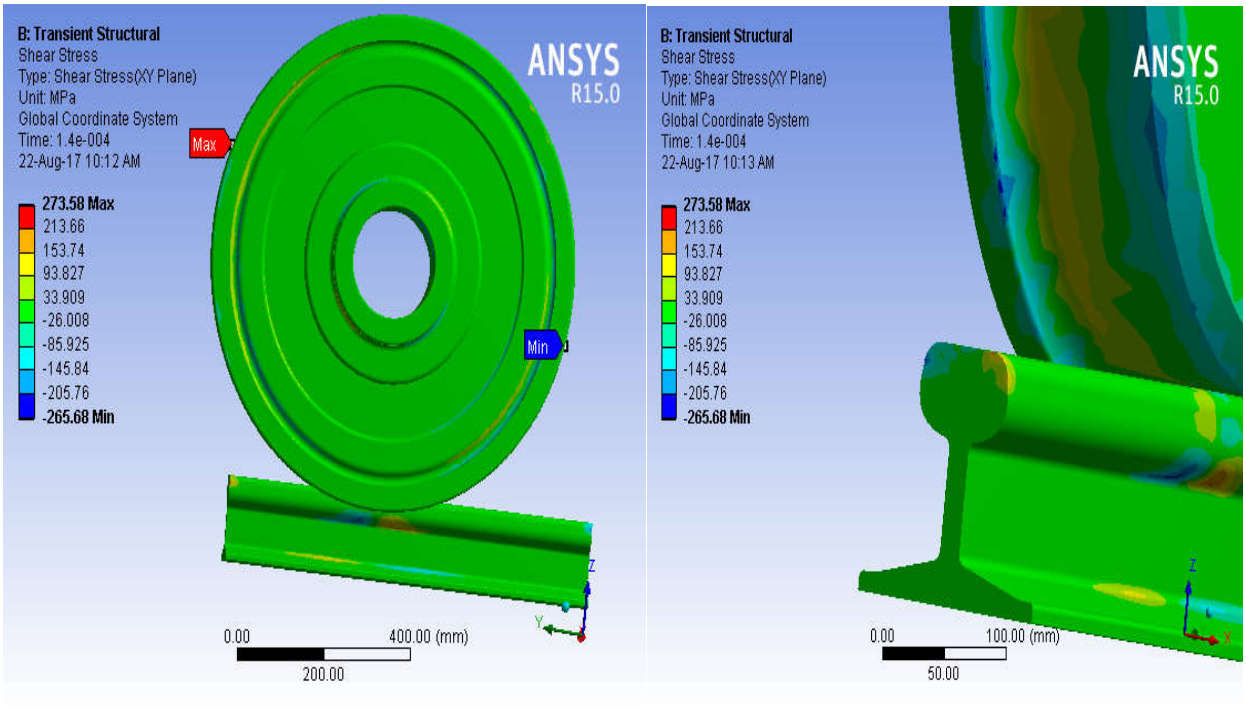

Figure 39 : Shear stress at 4m/s sliding velocity and traction coefficient of μ=0.58 simulation

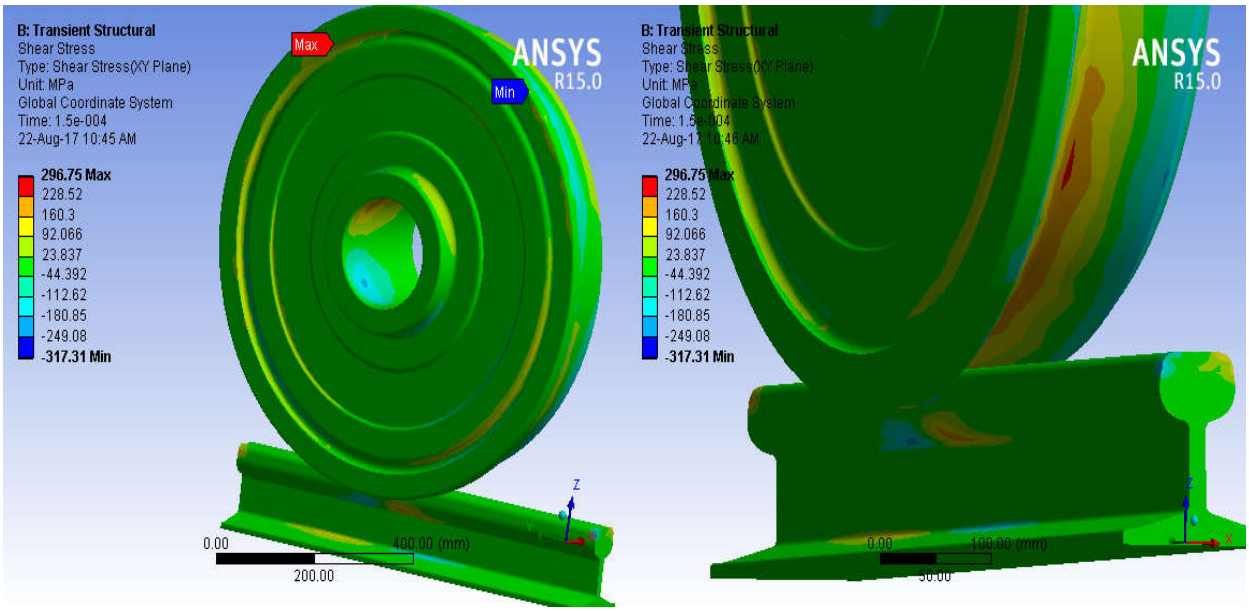

Figure 40 : Shear stress at 8m/s sliding velocity traction coefficient at μ=0.5 simulation

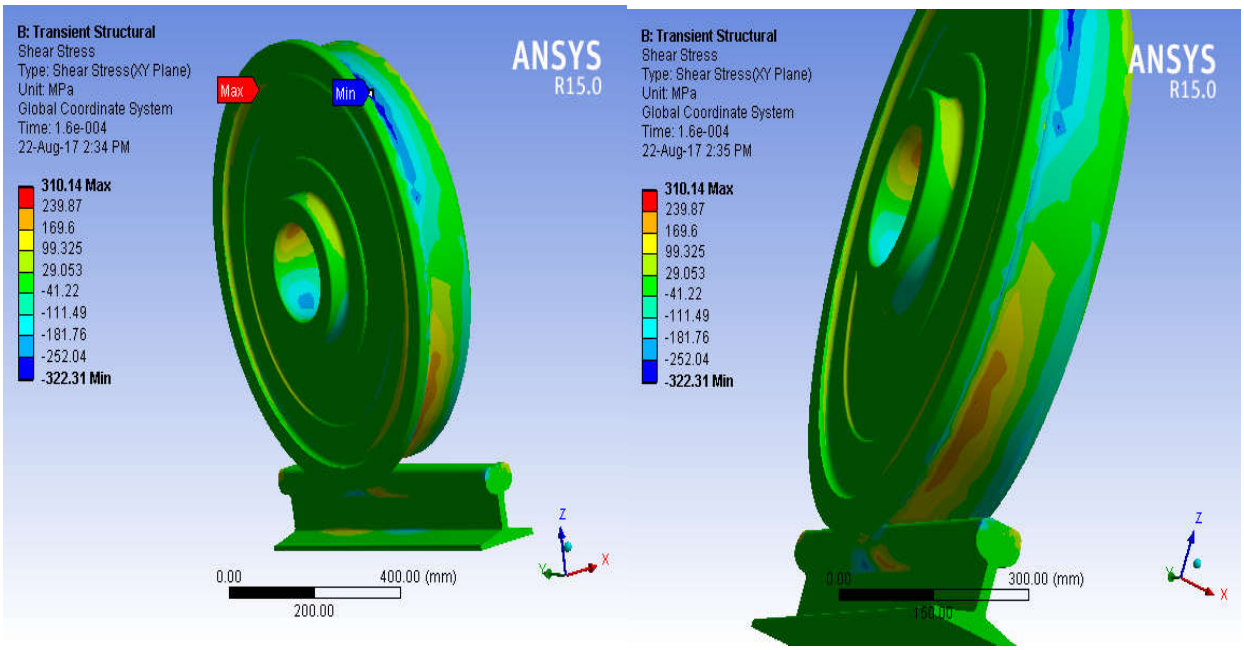

Figure 41 : Shear stress at 12 m/s sliding velocity traction coefficient of μ=0.4 simulation

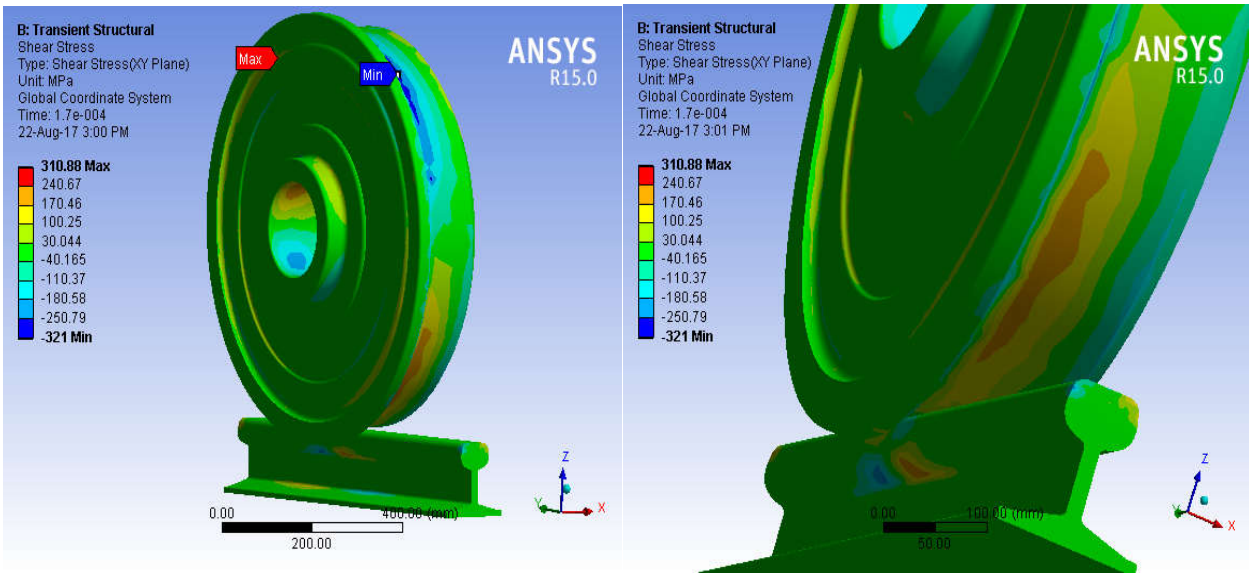

Figure 42 : Shear stress at 16 m/s sliding velocity traction coefficient of μ=0.3 simulation

If the wheel and the rail are initially at the ambient temperature, the thermal stresses due to frictional heating are equal in both of them. But the distribution of equivalent stress is no longer the same in all cases because of the couple mechanical and thermal stresses. This will cause thermal stress development on sliding contact area. The source of heat generation at the contact area between rail and wheel is friction force. The slip between wheel and rail causes frictional heating of both bodies. The maximum surface temperature during rolling contact of railway wheels with sliding friction is estimated using Blok's flash temperature formula [19]. In addition for determining temperature rise of these components, the heat partition factor of rail and wheel is added on analysis. The results can be summarized in the following Tables

Table 7: Result summary of heat flux and max temperature at rail surface

Traction coefficient	**0.58**	**0.5**	**0.4**	**0.3**
Sliding velocity	4	8	12	16
Heat flux	408	720	877	894
Rail surface temperature	866	1522	1863	1898

Table 8: Result summary of heat flux and max temperature at wheel surface

Traction coefficient	0.58	0.5	0.4	0.3
Sliding velocity	4	8	12	16
Heat flux	408	686	811	841

wheel surface temperature	788	1231	1246	11352

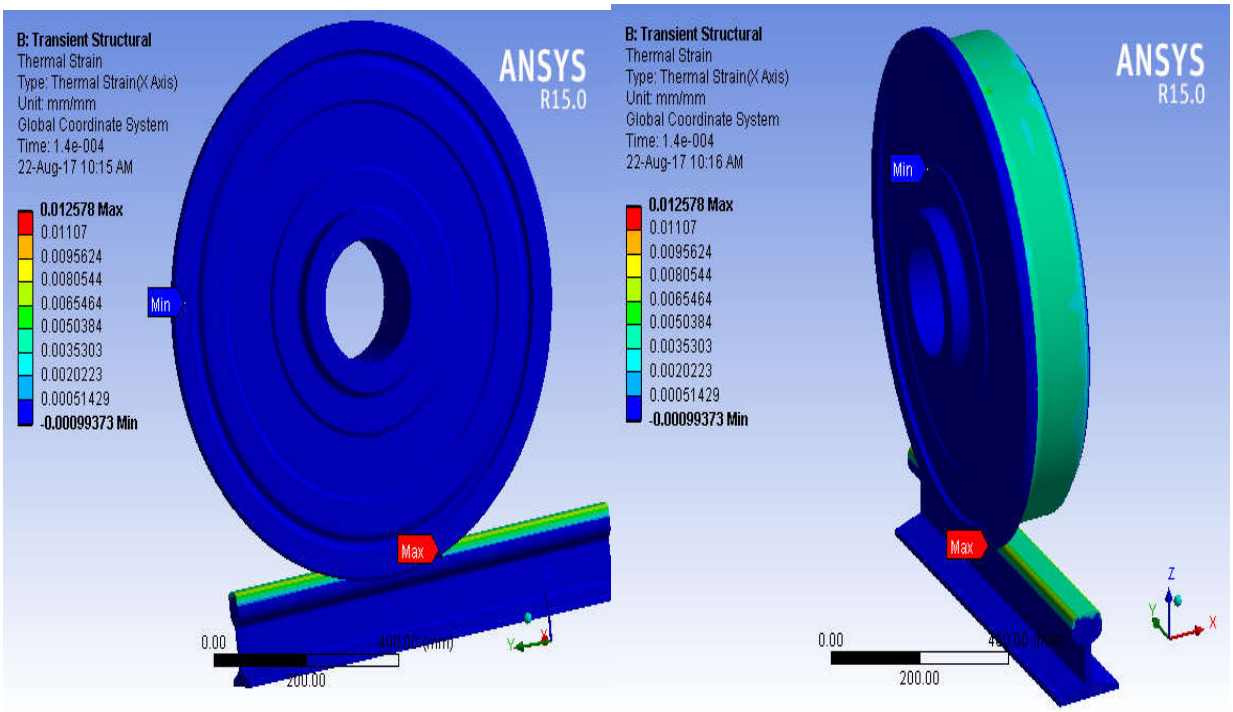

Figure 43 : Thermal strain at 4 m/s slip velocity traction coefficient of μ=0.58 simulation

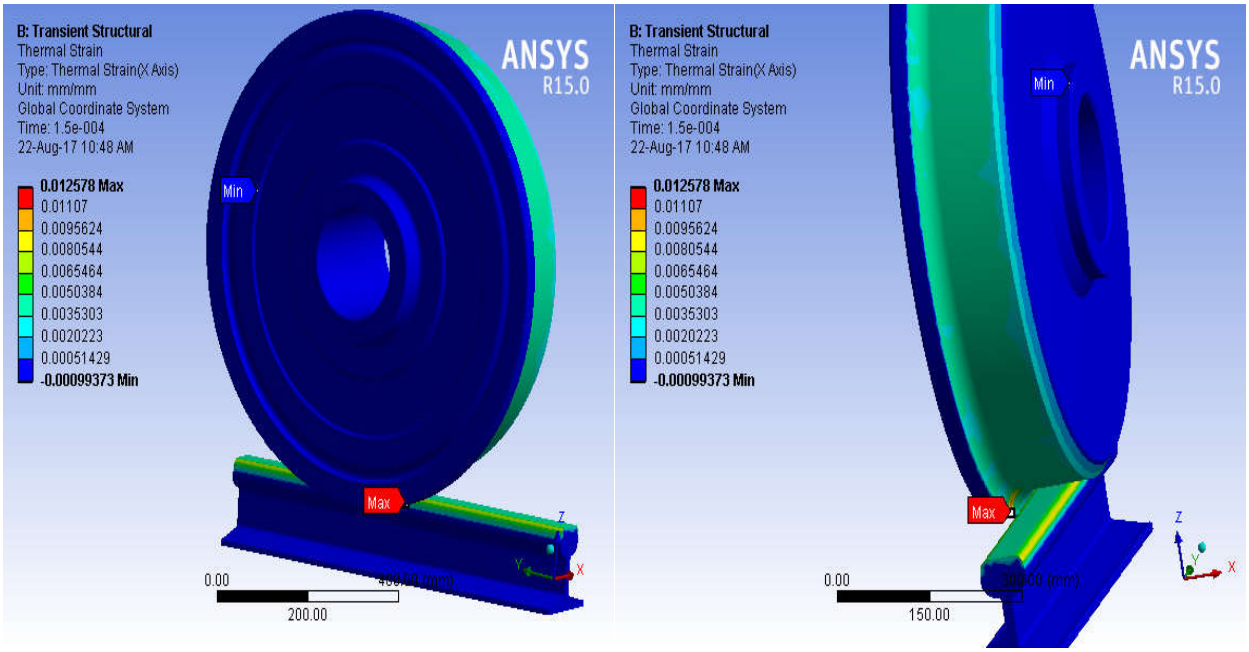

Figure 44 **:** Thermal strain at 8 m/s sliding velocity and traction coefficient of μ=0.5 simulation

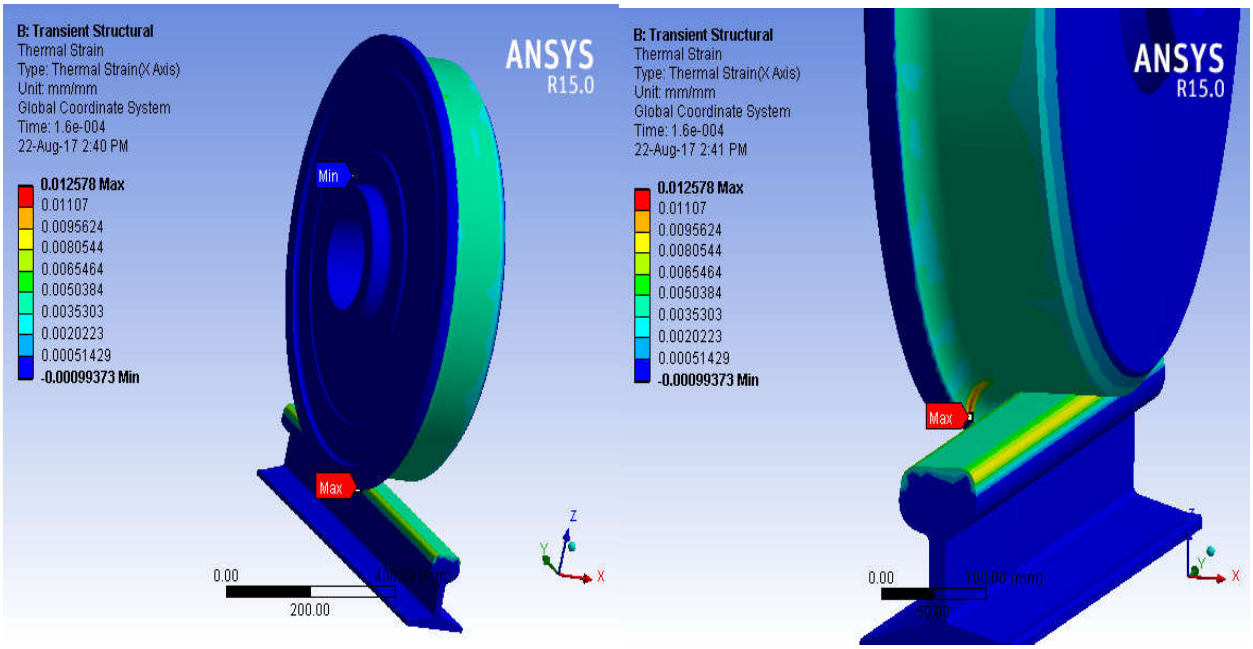

Figure 45 : Thermal strain at 12 m/s sliding velocity and traction coefficient of μ=0.4 simulation

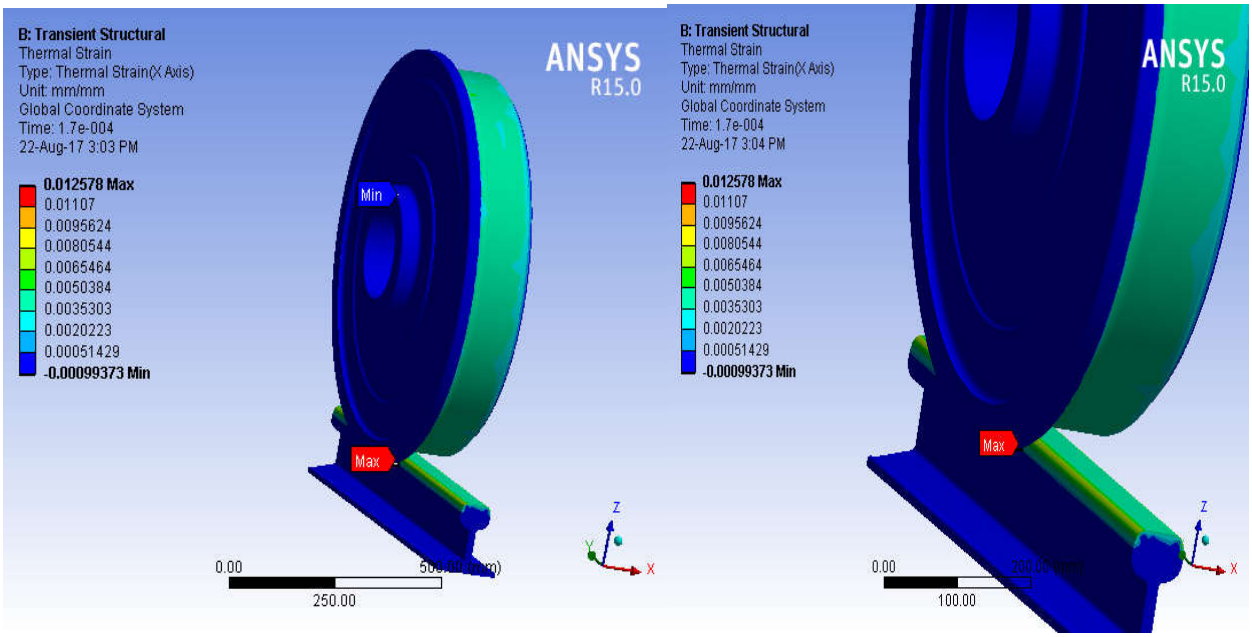

Figure 46 : Thermal strain at 16 m/s sliding velocity traction coefficient of μ=0.3 simulation

6.1.4 Loading Type

Fatigue, by definition, is caused by changing the load on a component over time. Thus, unlike the static stress safety tools, which perform calculations for a single stress, fatigue damage occurs when the stress at a point changes over time. ANSYS can perform fatigue calculations and analysis for either constant amplitude loading or proportional non-constant amplitude loading.

A scale factor can be applied to the base loading if desired. This option, located under the "Loading" section in the details view, is useful to see the effects of different finite element load magnitudes without having to re-run the stress analysis.

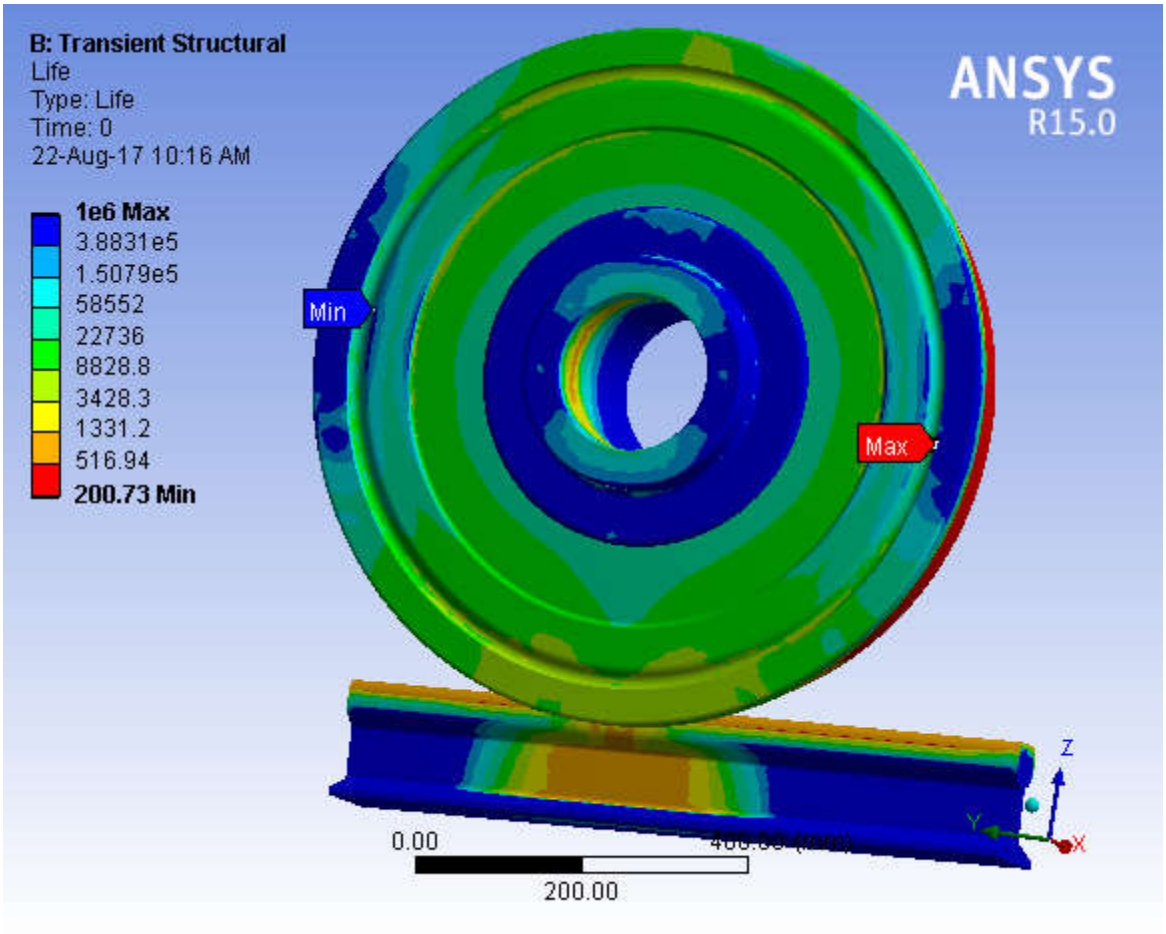

Figure 47 : Stress life at contact area of at 4 m/s sliding velocity and traction coefficient of μ=0.58 simulation

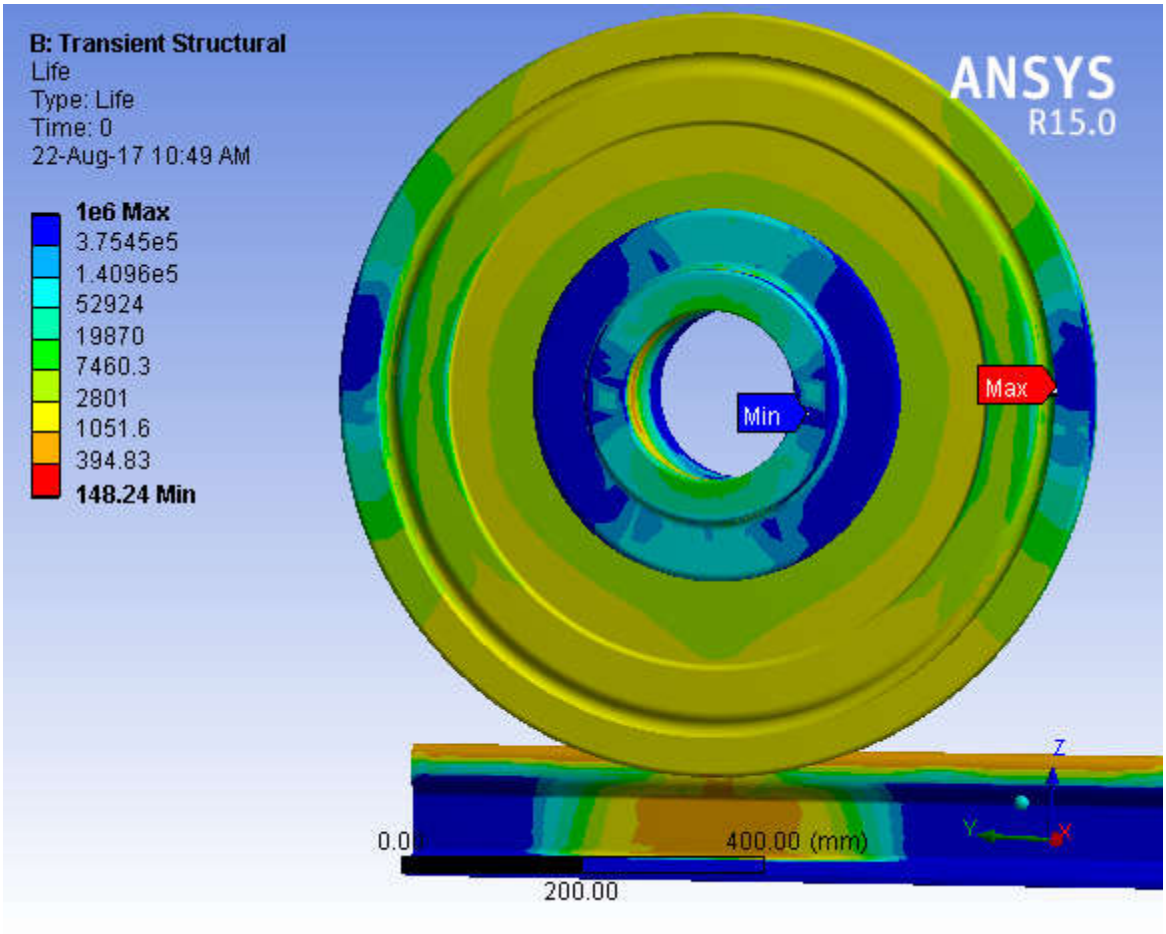

Figure 48 : Stress life at contact area at 8 m/s sliding velocity and traction coefficient of μ=0.5 simulation

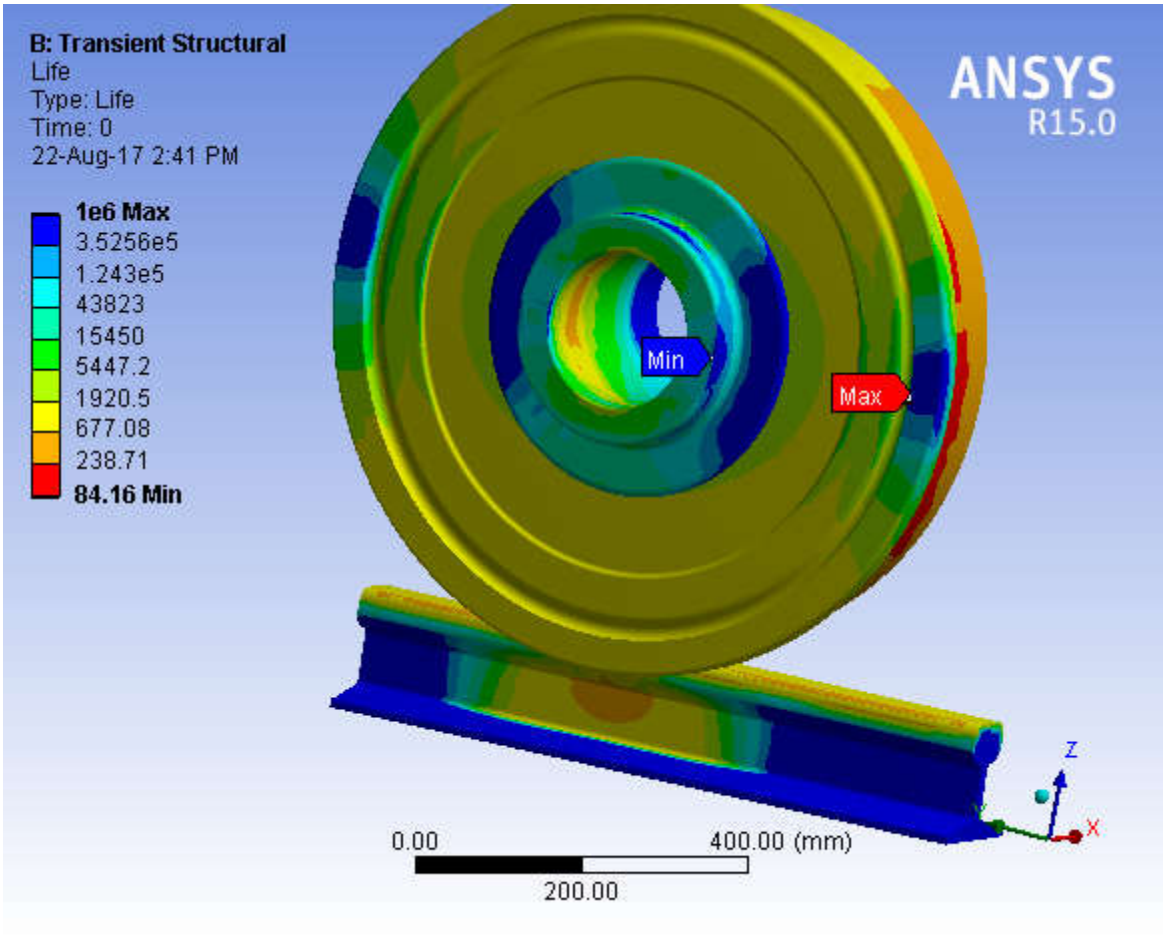

Figure 49 : Stress life at contact area of 12 m/s sliding velocity and traction coefficient of μ=0.4 simulation

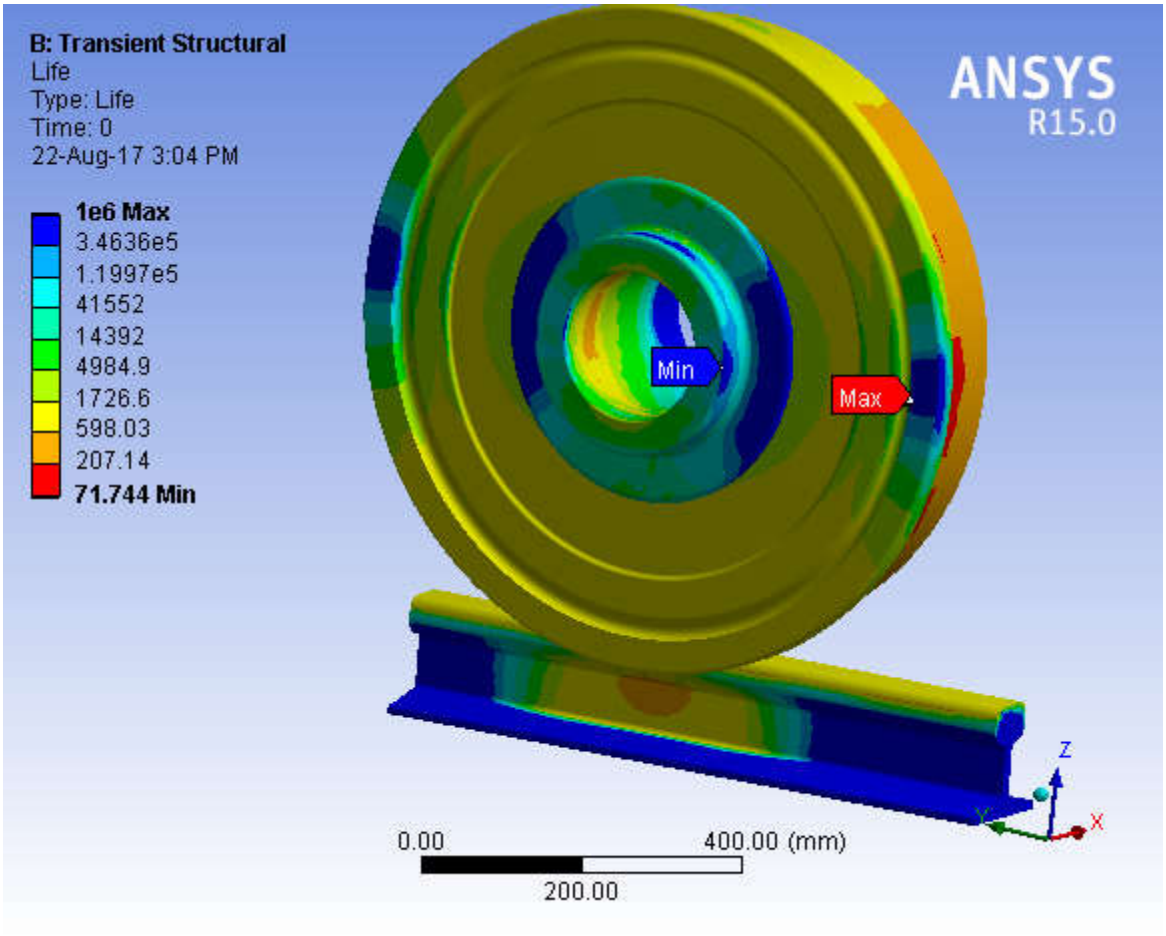

Figure 50 : Stress life at contact area of 16 m/s sliding velocity and traction coefficient of μ=0.3 simulation

Stress life analysis is one of indication of the effect loads on rail and wheel material. Contour plot results showing the number of cycles until failure due to fatigue. Additionally Gerber mean stress correction theory provides good fit for ductile metals for tensile mean stresses, although it incorrectly predicts a harmful effect of compressive mean stresses, as shown on the left side of the graph

$$\frac{\sigma_{alt}}{S_{end-limit}} + \left(\frac{\sigma_{means}}{S_{ult-strength}}\right)^2 = 1$$

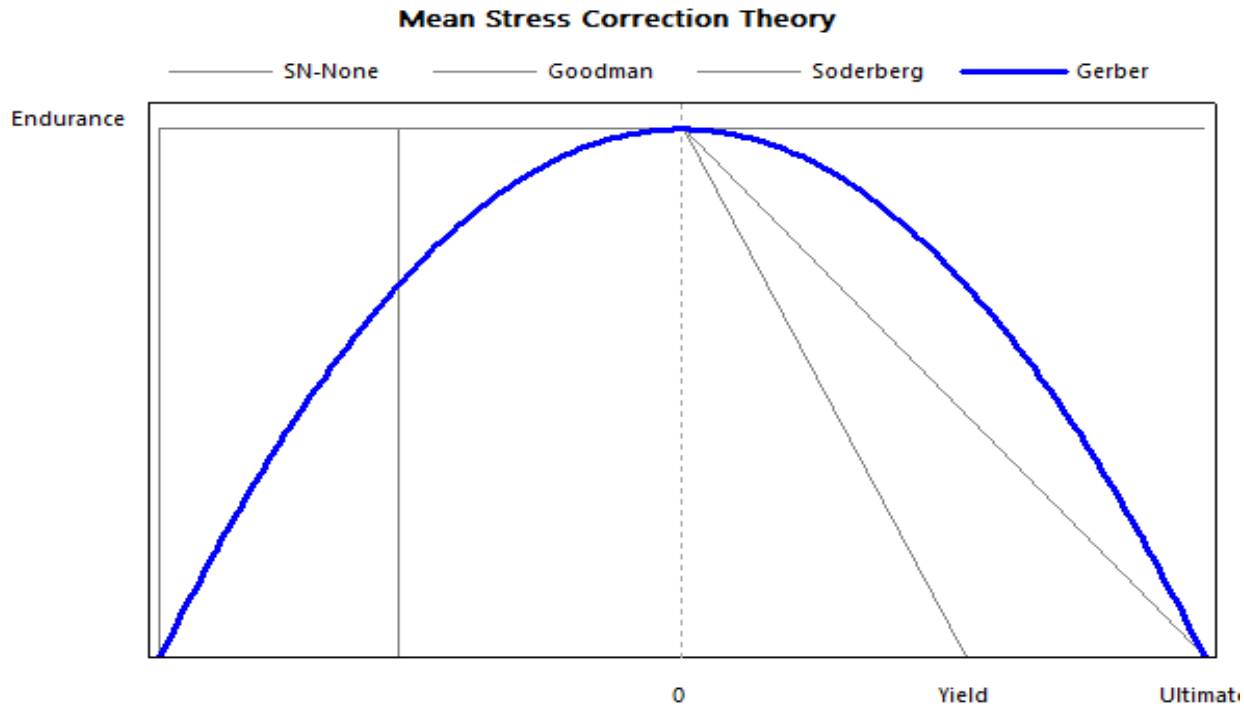

Figure 51 : Equation and graphical representation of the Gerber Mean Stress Correction for Stress Life Fatigue Analysis.

6.1.5 Stress-Life (S-N)

Fatigue material data stored as tabular alternating stress vs. life points. The ability to define mean stress dependent or multiple r-ratio curves if the data is available. Options to have log-log, semi-log, or linear interpolation. Mean stress effects in fatigue are usually presented as stress amplitude versus mean stress plot. For a particular given cyclic life it is usually observed that the load amplitude of the endurance limits decreases with growing mean stress or static load.

Stress life (S-N) Curve that show the relationship of stress amplitude to cycles to failure plotted bellow.

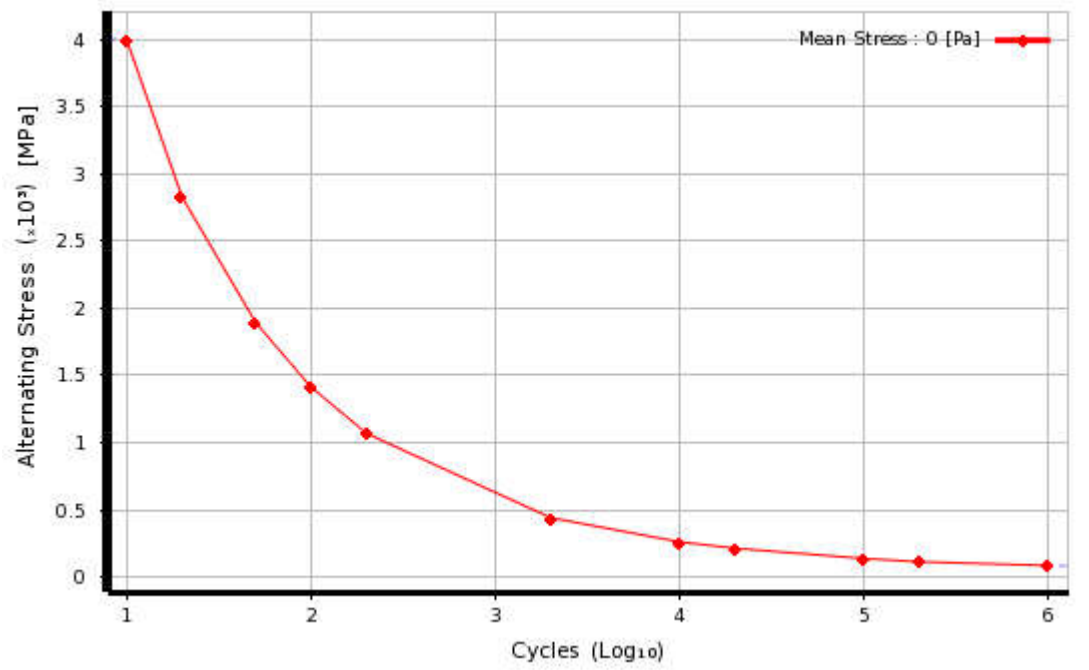

Figure 52 : The Stress-Life (S-N) Curve draw to logarithmic plot.

6.2 Discussion

The element is capable of giving plastic stress output for the loads beyond elastic limit. The normal and tangential stresses together with high thermally stresses may lead to higher levels of plastic deformation when compared to case with only the mechanical loads. A wheel sliding on a rail may cause severe thermal damage on the rail surface. The working hardening properties exhibits the plasticity and nonlinear response of the material.

1

Table 9 : The value of maximum elastic and plastic strain from combined loads.

Sliding velocity	Traction coefficient	Max. elastic strain	Max. plastic strain
4 m/s	0.58	0.005432	0.032213
8 m/s	0.5	0.0064024	0.044474
12 m/s	0.4	0.0077223	0.060074
16 m/s	0.3	0.0082628	0.066665

The frictional heat source generated by wheel-rail rolling/sliding contact is simulated by the flux boundary condition. As heat flux and maximum pressure applied due to rolling –sliding at contact area increase the effect that impose on contact area and also it reduces the strength of wheel and rail on whole bodies. ANSYS is used to simulate the loading and boundary conditions of the rail and wheel contact for a coupled analysis.

As the loads due to slippage at contact area increase the effect that impose on contact are also increase as we can notice from pictorial graphs presented above. Few micro second slippages create large amount of stress and strain. For the four case of analysis the results are presented the following tables for comparison.

Table 10 : Comparison of maximum equivalent thermal stress and combined stress

Sliding velocity	Traction coefficient	Thermal stress (MPa)	Combined stress (MPa)
4 m/s	0.58	975	1067.5
8 m/s	0.5	973.96	1409.4
12 m/s	0.4	973.03	1529.2

16 m/s	0.3	972.22	1626.7

The equivalent stress in combined load is the sum of the stress created mechanical and thermal load so its value is high form individual stress. Almost for the four case of simulation equivalent stress is higher than yield strength of the material

Table 11 : the maximum shear strain with varying sliding velocity and at different traction coefficient

Sliding velocity	Traction coefficient	Max. shear stress
4 m/s	0.58	271.58
8 m/s	0.5	296.75
12 m/s	0.4	310.14
16 m/s	0.3	310.88

As seen from result table above, by increasing traction coefficient, the shear strain between rail and wheel increase and it lead to cause fatigue on wheel rail material. Since increasing sliding/slip velocity and traction coefficient in time second the stress maximum caused by thermal expansion and mechanical contact conditions exceeds the yield strength, shear strain appears on and under the wheel and rail. Due to the wheel sliding on the new surface of rail, it induced more heat generate by cause of friction occur between wheel rail during rolling- sliding contact.

Table 12: Comparison of minimum stress life during combined loads condition

Sliding velocity	Traction coefficient	Min. stress life
4 m/s	0.58	200.73
8 m/s	0.5	148.24

12 m/s	0.4	84.16
16 m/s	0.3	71.744

The stress life is very small for high value slippage which can results low cyclic fatigue. Stress life due to mechanical load is 2.8 times higher than stress life during 4 m/s sliding velocity. Referring from the result above with increasing sliding velocity and decreasing of traction coefficient the life stress decrease to more minimum. This is because of existence of thermal load on contact area.

CHAPTER SEVEN

7.1 CONCLUSION AND RECOMMENDATION

7.1.1 Conclusion

The thesis presents analysis coupling of thermomechanical of wheel – rail rolling- sliding contact. A three dimensional finite element model is used for the mechanical –thermal coupling of wheel-rail rolling contact analysis. The assembly of wheel-rail geometry is created by CATIA V5R20 software. The finite element program ANSYS workbench is used to model the couple of thermo-mechanical rolling –sliding contact analysis and used to simulate the loading and boundary conditions of the wheel-rail rolling/sliding contact. However varying the traction coefficient and sliding velocity condition from low to high can cause significant changes to the stick/slip region, traction force, and tangential stress components. The distribution of the heat flux of wheel and rail was inputted by tabular data along contact area. Thermal stress and strain induced due to friction heat during slippage create challenge on the strength of the rail and wheel material. This model enabled the investigation of real-life contact conditions. The results so obtained show that each of the two different loads are applied at the contact and their characteristic variations over time act in contact of two body create conditions that promote the appearance and propagation of cracks and material fatigue problems. Taking into consideration that the contact pressure and the thermal stresses express their negative impacts in different positions of the contact zone. Since the stress maximum caused by thermal expansion and contact conditions exceeds the yield strength, plastic strain appears on and under the wheel tread. As seen that on and under the surface compressive and tensile stresses followed each other, the same way as in the tread warming up and cooling down phase. Distribution of pressure, surface shear stress and micro –slip in wheel –rail rolling – sliding contact occurred. Based on analytical analysis results, temperature increase and increasing traction coefficient to extreme values when sliding velocity increase indefinitely.

7.1.2 Recommendation

In present paper to analyze couple of mechanical – thermal using analytical and numerical modeling of thermal and mechanical wheel - rail rolling sliding contact. Hence, the recommendation from the analysis result are as follow.

The main cause of thermal and mechanical load at contact area is wheel sliding/rolling .Sliding is a well know problem in rail way industries and should need to be control in order to minimize thermal loads and low cyclic fatigue of rail- wheel material. High amount of heat can be generating from contact slippage special if axle lock happed during train startup time or decelerating near stations. Cooling mechanism is required in order to reduce contact temperature. Surface temperature above the melting point of the material is predicated through theoretical analysis. If this let to happen, the rail surface will burn and cause rail brakeage especially for full slippage (0.58) situation. Beside, timely clearing rails from dirty material and contaminate is helpful in controlling slippage. Now days, most locomotive are equipped with automatic anti-slip controllers. The efficiency and effectiveness of Ethiopian railway cars anti slip controller's facility should be tested timely .The severity of the effect of slippage high in the time for braking than during traction. The driver should be alert for controlling wheel slippage especially during applying brake. Preventive maintenance through timely re-profiling of rail and wheel is important order to reduce slippery surfaces. Specific service distance for re-profiling should be allowed. In the mechanical part, the 3D transient FE model is able to solve both the normal and the tangential contact problems simultaneously for arbitrary wheel-rail geometries. Finally timely supervising and selecting appropriate material which have high strength and resist thermal and mechanical load is needed to be considered for longer life and safe operation of railway system.

7.1.3 Future work

The scope of the present thesis focus on the couple of thermomechanical analysis rolling-sliding contact at the wheel-rail interface using finite element analysis ANSYS software. The couple analysis is based on the stress, strain, heat flux, fatigue life approach and by considering maximum pressure effect during wheel - rail contact. The couple analysis is performed by applying the mechanical loads and heat generate to the wheel-rail contact at different traction coefficient and different slip velocity. The continuity of the thesis work will be:

To improve the accuracy and applicability of the developed method, the following extensions can be formulated and suggested

- The present thesis attempted to predict the fatigue at the wheel-rail rolling contact at different traction coefficient (i.e. 0.2, 0.3, 0.4, 0.5, 0.58) and different slip velocity (i.e. 3, 6, 9, 12, 15) using ANSYS software and it enable to oversees the effect of pressure and heat flux at the wheel-rail rolling –sliding contact. Therefore, the results obtained from the FEA should be check experimentally using appropriate testing machine.
- In the current computations, the models can only be used for Hertzian normal contacts. To extend the solution to the whole wheel-rail contact range (also including non-Hertzian contact cases.
- Furthermore, the geometry and the initial input data need to be parametrized to allow the standard everyday use of this computation method for design solutions (e.g.: WSP development) and to enable simulating different wheels, sliding environments, etc.
- FE analysis of low cyclic fatigue and profile change and wear of rail-wheel materials during slippage by using the full licensed software.
- There is a lack of ultrasonic technique which used to determine the shape and size of the contact area
- The result was more visible if the material properties of wheel and rail were selected from different materials. Due to this any interested researcher could perform further analysis wheel-rail contact from different material.

8. REFERENCES

[1] Pankhurst, R. (1963). The Franco-Ethiopian Railway and Its History. *Ethiopia Observer*, *6*(4), 342-379.

[2] Crozet, Jean-Pierre. Françoise Faulkner-Trine, trans. The Franco-Ethiopian and DjiboutoEthiopian Railway and "History". 2013. Accessed 12 Feb 2014

[3] Ethiosports, Track laying commences on section of Ethio-Djibouti Railway project, Published By Markos Berhanu On Sunday, May 11th 2014

[4] Corporation discloses/Addis light rail project detail". The Ethiopian Herald. 10 March 2013. Archived from the original on 2013-03-11. Retrieved 2014-10-25.

[5] Uhlig, M. (2013). ESR0330 Wheel defect manual. Engineering standard rolling stock, 1.

[6] Zwierczyk, P. T. (2015). Thermal and stress analysis of a railway wheel-rail rolling-sliding contact.

[7] Abdulmenan Sulti. Thermal and stress analysis of AALRT wheel when braking with block brake", Addis Ababa University Institute of Technology School of Mechanical and Industrial Engineering, (2014)

[8] Zhao, X., Jin, X., & Zhai, W. (2007). Analysis of thermal-elastic stress of wheel-rail in rolling-sliding contact. *Chinese Journal of Mechanical Engineering(English Edition)*, *20*(3), 18-23.

[9] Tanvir, M. A. (1980). Temperature rise due to slip between wheel and rail—an analytical solution for hertzian contact. *Wear*, *61*(2), 295-308

[10] Hertz, H. (1882). Über die Berührung fester elastischer Körper. *Journal für die reine und angewandte Mathematik*, *92*, 156-171.

[11] Abbasi, U. O. Y. Z. S., & Lewis, R. L. S. Tribology of the wheel-rail contact–aspects of wear, particle emission and adhesion.

[12] Johnson, K. L., & Johnson, K. L. (1987). *Contact mechanics*. Cambridge university press.

[13] Knothe, K., & Liebelt, S. (1995). Determination of temperatures for sliding contact with applications for wheel-rail systems. *Wear*, *189*(1-2), 91-99.

[14] Ertz, M., & Knothe, K. (2002). A comparison of analytical and numerical methods for the calculation of temperatures in wheel/rail contact. *Wear*, *253*(3), 498-508.

[15] Haidari, A., & Hosseini-Tehrani, P. (2014). Fatigue analysis of Railway wheels under combined thermal and mechanical loads. *Journal of Thermal Stresses*, *37*(1), 34-50.

[16] Fischer, F. D., Werner, E., & Yan, W. Y. (1997). Thermal stresses for frictional contact in wheel-rail systems. *Wear*, *211*(2), 156-163.

[17] Ramanan, L., Kumar, R. K., & Sriraman, R. (1999). Thermo-mechanical finite element analysis of a rail wheel. *International journal of mechanical sciences*, *41*(4-5), 487-505

[18] Zhao, X., & Li, Z. (2011). The solution of frictional wheel–rail rolling contact with a 3D transient finite element model: Validation and error analysis. *Wear*, *271*(1), 444-452.

[19] Blok, H. (1937). Theoretical study of temperature rise at surfaces of actual contact under oiliness lubricating conditions. *Proc. Instn. Mech. Engrs.(General discussion on lubrication and lubricants)*, *2*, 222.

[20] STANDARD, B. (2007). *Railway applications—Wheelsets and bogies—Wheelsets—Products requirements* (Doctoral dissertation, Korea Railroad Research Institute)

[21] Johnson, K. L. Contact Mechanics, Cambridge University Press, Cambridge, 1985.

[22] Boussinesq, J. (1885). *Application des potentiels à l'étude de l'équilibre et du mouvement des solides élastiques: principalement au calcul des déformations et des pressions que produisent, dans ces solides, des efforts quelconques exercés sur une petite partie de leur surface ou de leur intérieur: mémoire suivi de notes étendues sur divers points de physique, mathematique et d'analyse* (Vol. 4). Gauthier-Villars

Zwierczyk, P. T. (2015). Thermal and stress analysis of a railway wheel-rail rolling-sliding contact.

[23] Yan, W., & Fischer, F. D. (2000). Applicability of the Hertz contact theory to rail-wheel contact problems. *Archive of Applied Mechanics*, *70*(4), 255-268

[24] Zong, N., & Dhanasekar, M. (2012). Analysis of rail ends under wheel contact loading. *International Journal of Aerospace and Mechanical Engineering*, *6*, 452-460.

[25] Anyakwo, A., Pislaru, C., & Ball, A. (2012). A new method for modelling and simulation of the dynamic behaviour of the wheel-rail contact. *International Journal of Automation and Computing*, *9*(3), 237-247.

[26] EN, T. (2011). 13674-1): Railway applications–track–rail–part 1: Vignole railway rails 46 kg/m and above.

[27] Grieve, D.G., Barton, D.C., Crolla, D.A. and Buckingham, J.T., „Design of a Lightweight Automotive Brake Disc using Finite Element and Taguchi Techniques“, Proc. Instn. Mech. Engrs, 212, Part D, 1998.